University of Alberta

Analysis of Dielectric Loaded Circular Waveguide Probes for Time Domain Reflectometry

by

Christopher Barry Reid Ryziuk

A thesis submitted to the Faculty of Graduate Studies and Research
in partial fulfillment of the requirements for the degree of

Master of Science

in

Electromagnetics and Microwaves

Department of Electrical and Computer Engineering

Spring 2014
Edmonton, Alberta

Abstract

Time domain reflectometry has been used for fluid level measurement and characterization since the 1960's, however, there is little research present in the literature to improve the measurements by using alternate probe designs. Numerical analysis of a dielectric loaded circular waveguide probe has determined that appropriately chosen dimensions and dielectric loading will allow for control of the reflection coefficient and consequently its permittivity accuracy. Additionally, the resulting reduction in signal velocity allows for an increase in height measurement accuracy. A detailed optimization procedure has been developed and implemented with MATLAB to determine the required probe dimensions and dielectric loading for a particular lossless application. Using Ansoft HFSS the validity of the lossless method was confirmed at low frequencies for lossy ethanol-water and acetic acid solutions. At 1GHz the procedure yields parameters that allow for accuracy increases on the order of 5 to 20 times that of a traditional probe.

Acknowledgements

I wish to express my deepest gratitude to my supervisor, Dr. Rambabu Karumudi, for providing me with this opportunity. His technical guidance, feedback and positive outlook have been of great importance during this work. I would also like to thank Kevin Chan for his technical support and guidance. In particular, his advice prior to my enrolment in this program was invaluable. Finally, I wish to thank my parents and Jenna for their endless support and sacrifice.

Contents

List of Figures

List of Tables

List of Symbols

$y(t)$	Input signal
$y_r(t)$	Received signal
$y_p(d,t)$	Dispersed signal
t	Time
t_1	Delay corresponding to the distance traveled in the air filled region of the probe
t_d	Delay corresponding to the distance traveled in the liquid filled region of the probe
d	Distance to the liquid
h	Height of the liquid
L	Probe length
a	Radius of the dielectric loading
b	Outer radius of the probe
$h_{\min}$	Minimum height of the liquid
Γ	Reflection coefficient
T	Transmission coefficient
Z	Characteristic impedance
j	Imaginary unit

c	Speed of light in a vacuum (2.998×10^8 m/s)
v_g	Group velocity in a medium
$v_{\mathrm{g,Liq}}$	Velocity of the pulse in the liquid
$v_{\mathrm{g,Liq,Max}}$	Maximum velocity within the liquid
ϵ_r	Relative permittivity
ϵ_r'	Real component of the relative permittivity
ϵ_r''	Imaginary component of the relative permittivity
$\tan\delta$	Loss tangent
σ	Conductivity
$\epsilon_{\mathrm{r,Load}}$	Relative permittivity of the dielectric loading
$\epsilon_{\mathrm{r,Liq}}$	Relative permittivity of the liquid
$\epsilon_{\mathrm{r,Peak}}$	Relative permittivity of the liquid at which the accuracy is to be optimized
$\epsilon_{\mathrm{r,Max}}$	Maximum relative permittivity of the liquid considered
γ	Propagation constant
α	Attenuation constant
β	Phase constant
β_0''	Second order approximation of dispersion
A_{disp}	Peak amplitude of a dispersed pulse
Γ_{disp}	Third order and higher dispersive effects on the reflection coefficient
t_{disp}	Third order and higher dispersive effects on the peak delay
μ	Permeability

μ_0	Permeability of free space ($4\pi \times 10^{-7}$ H/m)
ϵ	Permittivity
ϵ_0	Permittivity of free space (8.8542×10^{-12} F/m)
A_{Tp}	Pulse width definition
T_p	Pulse with duration
BW	Bandwidth
τ_0	Gaussian pulse width
τ	Dispersed Gaussian pulse width
$Y(f)$	Fourier transform of the signal
ω	Angular frequency
f	Frequency
f_{car}	Carrier frequency
$f_{c,01}$	Cutoff frequency of the TE_{01} mode in the air filled region of the probe
$f_{c,02}$	Cutoff frequency of the TE_{02} mode in the liquid filled region of the probe at the maximum liquid permittivity considered
$F(\gamma)$	Characteristic equation
E	Electric field
H	Magnetic field
$J(x)$	Bessel function of the first kind
$N(x)$	Bessel function of the second kind
k	Wave number
n	Angular variation of the fields

m	Radial variation of the fields
∂h	Error in height measurement
$\partial \epsilon_r$	Error in permittivity measurement
Δh	Height measurement accuracy increase in multiples of TEM
$\Delta \epsilon_r$	Permittivity measurement accuracy in multiples of TEM

List of Acronyms and Abbreviations

TEM	Transverse electromagnetic
TE	Transverse electric
TM	Transverse magnetic
HE	Hybrid electric
TDR	Time domain reflectometry
HFSS	High frequency structural simulator
VNA	Vector network analyzer

Chapter 1

Introduction

Time domain reflectometry (TDR) has become an accepted method for simultaneously measuring the level of liquid within a tank while also measuring the relative permittivity of the liquid. Cost efficient measurements can be made by using only the amplitude and delay of the received pulse. The permittivity can then be used to estimate properties of the fluid, including, composition, quality, concentration, density or water content. TDR for permittivity measurements has been in use since the 1960's [1], although the concept had been in use for fault detection for many years. Within the last two decades, TDR has been heavily utilized and researched for soil moisture content. In recent years, very fast pulse repetition times have allowed TDR to become a practical and cost effective means to monitor height and permittivity changes in real time for industrial process control applications. This thesis explores the feasibility of utilizing a dielectric loaded circular waveguide probe to have greater control over its signal propagation and reflection properties, thereby allowing for a significant increase in accuracy over conventional probes.

1.1 Literature Review

A review of the state of the existing literature relative to TDR, fluid level, and permittivity measurement applications has been given in this Section. Although the focus of this thesis is on fluid level and its material characterization using TDR, it is more popularly used in soil measurement and fault location applications. A brief review of the other TDR applications is given in Section 1.1.1. The competing microwave methods for determining liquid level and the permittivity of materials are summarized in Section 1.1.2. The literature rel-

evant to liquid level and material characterization has been given in Section 1.1.3.

1.1.1 Other TDR Applications

Determining soil water content has traditionally been one of the most common applications of TDR [2, 3]. A detailed review of the advances in measurement of the dielectric and electrical conductivity of soils has been prepared in [4, 5, 6]. Various probe designs have been studied to alter the field configuration which can result in an improved spatial sensitivity. Single rod [7], two wire, three wire, seven wire, coaxial, parallel plate and dielectric coated probes have been investigated [6, 8, 9]. For example, single rod probes were shown to have an increased sensitivity over two rod probes due to the circular symmetry. A dielectric coating with relative permittivity of approximately 35 was found to increase sensitivity measurements of very lossy soils where the signal would otherwise be attenuated. The measurement of soil water content typically uses a probe that penetrates into the soil, however, it has been shown that noninvasive methods can be used that allow for measurement of the water content of pavement, hard rock drill cores, or hardened soil [10]. Recently, a coiled probe has been designed to measure the Matric potential of soil. The Matric potential is a soil property that is a combined measure of the capillary and absorptive forces of soil particles [11].

In recent years TDR has been applied to a wide range of applications. The moisture content in rice and its dielectric relaxation curves have been found [12]. TDR has been used as a method to locate discontinuities and to monitor water trees on power cables [13], or to monitor the integrity of pipelines [14]. Application specific probes have been proposed that allow for landslide detection [15], obstacle detection [16] or pressure measurement [17]. TDR has also been used to measure the characteristic impedance of nonuniform transmission lines [18].

1.1.2 Alternate Measurement Methods

A review of the available microwave techniques to measure the dielectric properties of polar liquids has been prepared by [19]. The complex permittivity of a material can be found by measuring the reflected and transmitted

signal. This can be done using either free space [20] or waveguide [21, 22, 23] based methods. The permittivity can also be determined by filling a waveguide with the liquid sample and measuring the change in cutoff frequency [24, 25]. Typically, a sample of known dimensions is prepared and frequency domain measurements are performed using a calibrated Vector Network Analyzer (VNA).

Time domain measurement methods will be covered in depth in the remainder of this thesis, however, frequency domain and time-frequency domain methods are also present in the literature. Frequency domain methods typically utilize either single or multiple continuous single frequency signals [26, 27, 28]. The minimum liquid thickness is determined by the attenuation of the liquid and the frequency separation of the signals. The system described in [27] reports a range error of ± 0.2mm, with the use of an HP-8510 network analyzer. Time-frequency domain based methods have reported an increase in fault detection [29] and permittivity measurement accuracy [30].

1.1.3 Applications of TDR for Liquid Characterization

This section will focus on liquid level and characterization applications. TDR was first proposed in the 1960's as a method to simultaneously characterize liquid properties and measure liquid levels. Time domain methods using amplitude based measurement, in conjunction with sequential sampling techniques [31], provide a cost effective alternative to frequency domain methods for industrial applications [32]. TDR has also been shown as a suitable method for monitoring liquid properties in real time [33].

The dielectric properties of a solution are typically proportional to its chemical composition, allowing for material properties to be inferred based on the measured dielectric properties. The fat content in milk and the freshness of the milk can be determined based on its dielectric properties [34, 35]. The resulting decrease in glucose during the fermentation process of Japanese sake has been shown to be related to its complex permittivity [36]. TDR has been used to measure the relaxation and thermodynamic behaviour of propylene glycol, it was found that the degree of polymerization is related to temperature and its complex permittivity [37]. The concentration of water based solutions such

as alcoholic beverages or acetic acid have been shown to be related to its complex permittivity [38, 39, 40].

TDR has been shown to perform favourably in most industrial environmental conditions. When compared to float, capacitive, ultrasonic and radar methods it performs well in most categories, including: dust, slurry, foam and agitation. However, it does not perform well in viscous, sticky or applications prone to encrustation [41]. Experiments have been performed by [42] to demonstrate the performance of TDR for real time measurement of liquid height and the dielectric properties of ethanol, acetone, fuel and diesel oil. The relative error in liquid level measurement was reported as 1.4% to 2.7% for liquid levels ranging from 12.5cm to 41.2cm. The relative error in permittivity measurement was reported to be less than 2%. De-ionized water has been studied in [43, 44] where a reported 2.1% error in relative permittivity measurement has been achieved.

Numerous probe designs have been proposed for soil measurement as discussed in Section 1.1.1, however, no literature related to alternate probe designs for the purpose of increased accuracy of permittivity or height measurement has been found. As will be discussed in the following sections, TDR probes typically utilizes TEM mode propagation which does not allow for such improvements. Two non-TEM structures, a dielectric rod and the Goubau waveguide, have been proposed in [45] for use with continuous wave liquid level measurement. It was found that these structures are less susceptible to deposits on the probe and the attenuation can be reduced. The Goubau waveguide and Sommerfeld wire (a Goubau waveguide without dielectric coating) have been studied for TDR applications [46, 7]. It was found that the region of influence of these probes is considerably larger and more symmetric than typical two-wire probes. A dielectric coating with relative permittivity up to 100 was studied, it was found that materials with high dielectric constant reduces the spatial sensitivity of the probe. Furthermore, it has been shown that a coiled probe can be used to reduce the impact of reflections from the end of the probe by increasing the distance the pulse travels [47].

1.2 Contributions of this Thesis

The primary focus of this thesis is the investigation of alternative probe configurations and their impact on fluid level monitoring and characterization applications. It was found that TEM mode structures, although established and widely used, cannot be customized further for particular applications. This resulted in the investigation of non-TEM mode structures, in particular the TE_{01} mode of a dielectric loaded circular waveguide. The propagation and reflection properties of waves utilizing these types of field configurations are extremely dependent on the geometry, frequency, and material composition of the probe. It has been found that this dependency allows for customization based on a specific application, thereby improving a variety of desirable properties, which is not possible using conventional TEM methods.

Non-TEM waves can be supported by a variety of structures. In this thesis, metallic waveguides will be studied in detail. At the desired frequency range, the size and strength of these structures are feasible for use in fluid level monitoring applications. The governing equations for dielectric loaded metallic waveguides have previously been studied in-depth, therefore derivations are not required as part of this work. However, the equations governing the field configurations are non-trivial transcendental equations. This required a detailed numeric solution strategy and optimization method to be developed for this work. This method has been implemented using MATALB. Liquid losses have been shown to have a detrimental impact on the reflection coefficient while significantly increasing the complexity and computational requirements of the solution procedure. As a result, low loss applications are preferred and losses have been omitted in the optimization procedure.

It has been found that dispersion is a significant drawback of non-TEM probes for measurement applications. Without diligent consideration given to the effects of dispersion, the impacts of pulse spreading would make non-TEM methods infeasible for measurement applications. The effects of dispersion have been well studied in fiber optic communication systems. Previously derived theory has been adapted in this thesis to allow for the use of these dispersive modes.

The performance of the optimized probe designs has been confirmed using Ansoft HFSS software. High permittivity applications were found to have the greatest potential for permittivity accuracy improvement. Multiple probe configurations have been provided for a range of liquid applications. To test the validity of the low loss assumption used in the optimization procedure, lossy ethanol-water and acetic acid solutions have been studied. At a carrier frequency of 1GHz it has been found that the lossless optimization routine can determine the dimensions and parameters of a probe for use in lossy applications.

Chapter 2

Principles of Time Domain Reflectometry

The basic theory required to measure the liquid permittivity and height using time domain reflectometry techniques will be described in this section. A typical setup used for these measurements is discussed in Section 2.1. The basic principals required to measure the height and liquid permittivity using TEM methods have been reviewed in Sections 2.2 and 2.3 respectively. The limitations that arise due to the presence of multiple reflections will be discussed in detail in Section 2.4. These limitations are often neglected due to attenuation or deemed insignificant because of small pulse widths. However, such simplifications are not applicable to the non-TEM methods proposed in this thesis. Consequently, a detailed method for determining the impact of multiple reflections on the above measurements has been developed. This method also allows for easy transition to the non-TEM methods discussed in the following Chapters.

2.1 Typical Measurement Setup

The TDR applications studied in this thesis are limited to the measurement of fluid level and material characterization, such as measuring the dielectric constant or concentration of the liquid solution. The experimental setup proposed in this thesis is shown in Figure 2.1. The probe illustrated in the figure provides a controllable means for which an electromagnetic pulse can interact with the liquid. The pulse is launched from the top of the guiding structure and is confined by the outer conducting walls as it propagates towards the liquid. Small perforations may be present on the exterior of the probe walls to

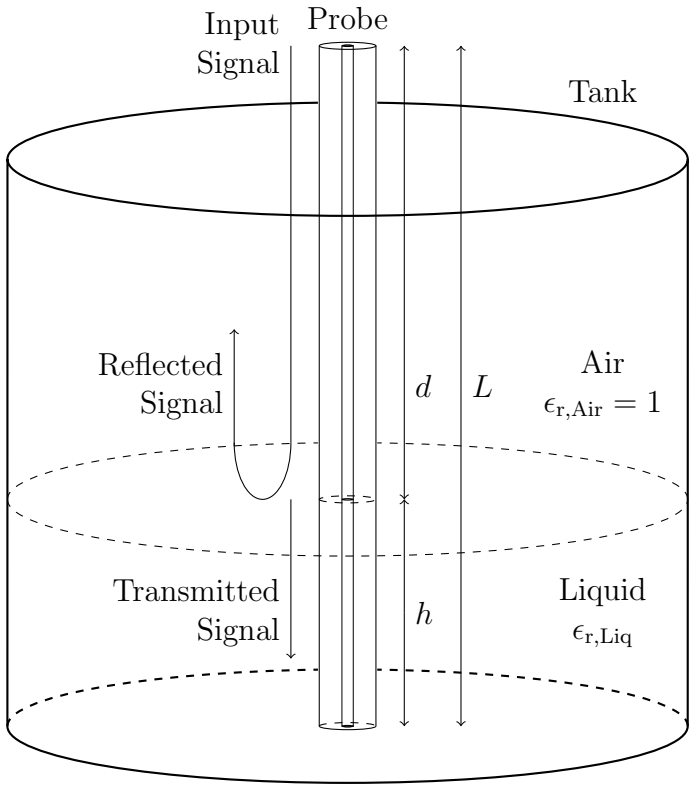

Figure 2.1: Typical experimental setup.

allow the liquid to easily pass into it. Provided that these holes are sufficiently small, they will not have a significant impact on the performance of the probe. The injected pulse travels down the probe a distance (d) towards the liquid with the group velocity (v_g) of the probe. Upon interaction with the liquid, the reflected signal is generated with amplitude proportional to the reflection coefficient (Γ). The remaining portion of the signal transmits into the liquid. The reflected signal then propagates back the same distance and velocity to the receiver. The reflected signal can modeled by,

$$y_r(t) \approx \Gamma y(t - t_1) \tag{2.1}$$

where $y(t)$ is the input signal and t_1 is the total delay introduced. In Section 2.2 it has been shown that this delay can be used to determine the height (h) of the liquid. Similarly, in Section 2.3 it has been shown that the amplitude can be used to determine the permittivity of the liquid.

The received signal modeled in Equation 2.1 is an approximation because

it neglects the impact of the portion of the signal that was transmitted into the liquid. This transmitted signal will continue to travel down the probe at the group velocity of the probe filled with the liquid ($v_{\mathrm{g,Liq}}$). The probe is typically terminated with a solid piece of metal which has a reflection coefficient of -1, although other terminations are possible. The signal reflected from the probe termination travels back along the probe to the liquid interface where a third reflection occurs. A portion of this signal will be reflected back into the liquid where this process repeats indefinitely while the remaining portion enters the air filled region of the probe and returns to the receiver. This phenomenon will be referred to as multiple reflections. The result is an infinite series of reflections that can cause errors in measurement. The conditions necessary to neglect these multiple reflections are discussed in detail in Section 2.4.

2.2 Propagation and Height Measurement

Fluid level measurement relies on the predictable nature of the speed of an electromagnetic wave in the guiding structure. In general, the group velocity of a TEM wave through a medium is known to be,

$$v_g = \frac{c}{\sqrt{\epsilon_r}} \tag{2.2}$$

Where c is the speed of light in vacuum (2.998×10^8 m/s), and ϵ_r is the relative permittivity of the medium the wave is travelling in. The relative permittivity of air is approximately 1. The distance to the liquid level interface can be found using the total delay between the launched and received time of the reflected pulse. The speed at which the signal travels is known from Equation 2.2, which results in,

$$d = \frac{v_g t_1}{2} \tag{2.3}$$

From this calculated distance and the known length of the probe, the liquid height can be determined,

$$h = L - d \tag{2.4}$$

2.3 Reflection and Permittivity Measurement

The magnitude of the reflection coefficient is defined as the ratio of reflected to incident signal amplitudes, and can be derived using either electromagnetic or impedance analysis. The latter will be used in this thesis as it provides a simple and intuitive method for comparing the reflection coefficient profile for various structures. Equations 2.5 to 2.12 are well known electromagnetic relationships as described in more detail by [48]. The reflection coefficient in terms of the characteristic impedance of the probe in the air and liquid filled regions of the probe is,

$$\Gamma = \frac{Z_2 - Z_1}{Z_2 + Z_1} \tag{2.5}$$

where Z_2 and Z_1 represent the characteristic impedance of the respective media filled portion of the probe. In our case Z_2 is the characteristic impedance of the probe within the liquid under test, while Z_1 is the characteristic impedance of the probe in air. Additionally, the transmission coefficient is defined in terms of the reflection coefficient,

$$T = 1 + \Gamma = \frac{2Z_2}{Z_2 + Z_1} \tag{2.6}$$

The impedance of a TEM wave is,

$$Z = \frac{j\omega\mu}{\gamma} \tag{2.7}$$

and γ is the complex propagation constant,

$$\gamma = j\omega\sqrt{\mu\epsilon_0\epsilon'(1 - j\tan\delta)} \tag{2.8}$$

The loss tangent ($\tan\delta$) is defined in terms of the real (ϵ') and imaginary component (ϵ'') of the dielectric constant ($\epsilon_r = \epsilon'_r + j\epsilon''_r$),

$$\tan\delta = \frac{\epsilon'_r}{\epsilon''_r} \tag{2.9}$$

and where,

$$\begin{array}{cc} \mu = \mu_r\mu_0 & \epsilon = \epsilon_r\epsilon_0 \\ \mu_0 = 4\pi \times 10^{-7}\ \text{H/m} & \epsilon_0 = 8.8542 \times 10^{-12}\ \text{F/m} \end{array} \tag{2.10}$$

The permeability (μ) is defined in terms of the free space permeability, (μ_0) and the relative permeability of the material (μ_r). Similarly, the permittivity is defined in terms of the free space permittivity (ϵ_0) and the relative permittivity of the material (ϵ_r). For typical TDR applications $\mu_r = 1$ and in air $\epsilon_r = 1$. Applying the results of Equations 2.5 to 2.10 yields the complex valued reflection coefficient of a TEM wave for a lossy liquid,

$$\Gamma = \frac{1 - \sqrt{\epsilon'_{r,2}(1 - j\tan\delta)}}{1 + \sqrt{\epsilon'_{r,2}(1 - j\tan\delta)}} \tag{2.11}$$

For low loss liquids $\tan\delta \approx 0$ which allows the complex component of the permittivity to be neglected. The reflection coefficient can then be written simply as,

$$\Gamma = \frac{1 - \sqrt{\epsilon_{r2}}}{1 - \sqrt{\epsilon_{r2}}} \tag{2.12}$$

Where ϵ_{r2} is the relative permittivity of the liquid under test. Note that the reflection coefficient is independent of the probe geometry for a TEM wave. The reflection coefficient over the range of relevant permittivity values is shown in Figure 2.2.

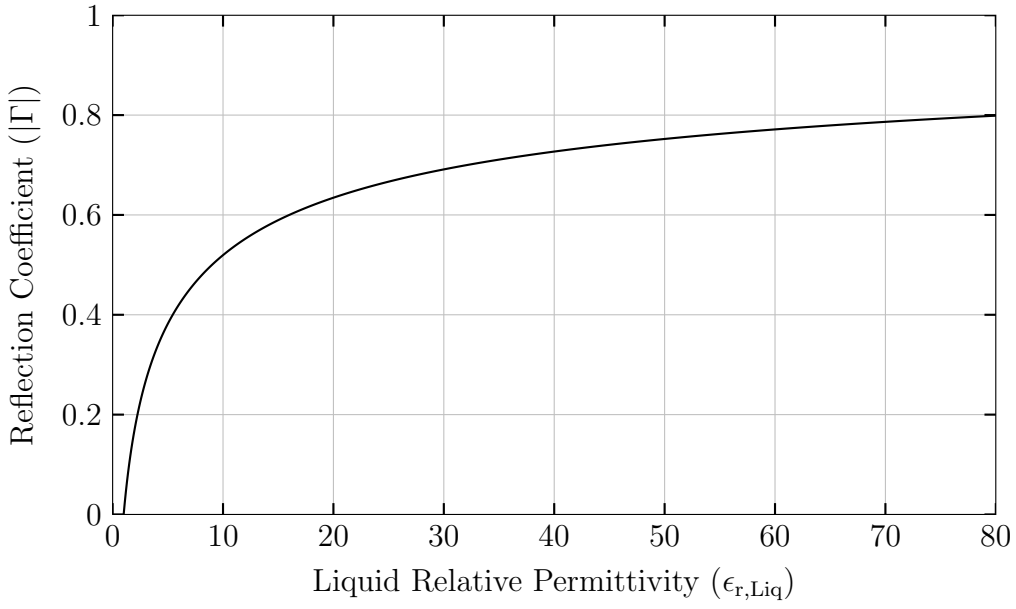

Figure 2.2: TEM reflection coefficient.

2.4 Pulse Width and Minimum Height

The minimum height ($h_{\min}$) is defined as the minimum required liquid height such that the subsequent reflected pulses do not cause significant error in the measurements. The minimum height is dictated by the pulse width used, the attenuation of the liquid, and the termination of the probe. For example, the pulse used in [38] has a rise time of 18ps which corresponds to a minimum height of less than 1cm. However, such a pulse would require significant bandwidth and is not suitable for dispersive waveguide applications. For liquids with significant attenuation the reflected pulses from the probe termination can be neglected [32]. Liquid losses will have a significant impact on the reflection properties of a waveguide probe, thus, liquids with low losses have been considered. Finally, the termination of the probe determines the magnitude of the subsequently reflected pulses. The probe can be terminated with either a short circuit, open circuit, or matched termination. A short circuit termination has been shown to provide more accurate results than the open ended type [49]. A matched termination can be used to absorb reflections but is not suitable for a large range of fluid permittivity values [45]. A short circuit termination has been used in this thesis. Careful consideration has been given to account for multiple reflections and to determine the required minimum height.

2.4.1 Pulse Width

The time domain pulse width (T_p) is defined for the purpose of this work as the point where the amplitude is reduced to the user defined value, A_{T_p}. It has been shown that this allows for a simple definition of minimum height and a direct correlation between A_{T_p} and the error introduced due to multiple reflections.

$$A_{T_p} \equiv \frac{y(T_p/2)}{y(0)} = \frac{Y(BW/2)}{Y(0)} \tag{2.13}$$

where BW is the bandwidth of the pulse and $y(t)$ and $Y(f)$ are the time and frequency representations of the Gaussian pulse. The Gaussian pulse is defined as,

$$y(t) = \exp\left(\frac{-t^2}{2\tau_0^2}\right) \tag{2.14}$$

Where τ_0 is the Gaussian pulse width. Solving for $y(Tp/2) = A_{T_p}$, setting $t = 0$, and rearranging gives the definition for the pulse duration that will be used in this thesis,

$$T_p = \tau_0 \sqrt{-8 \ln(A_{T_p})} \tag{2.15}$$

The same definition has been applied to bandwidth as this will determine the portion of the signal that is contained within the allotted frequency range. This will be of particular importance in the following chapter where this definition is utilized to determine the limit imposed by higher order modes. The frequency domain representation of a Gaussian signal is,

$$Y(f) = \tau_0 \sqrt{2\pi} \exp\left(\frac{-(2\pi f \tau_0)^2}{2}\right) \tag{2.16}$$

Solving for $Y(BW/2) = A_{T_p}$, setting $f = 0$, and rearranging, the bandwidth is,

$$BW = \frac{\sqrt{-2 \ln(A_{T_p})}}{\tau_0 \pi} = \frac{-4 \ln(A_{T_p})}{T_p \pi} \tag{2.17}$$

The above definitions are illustrated in Figures 2.3 and 2.4.

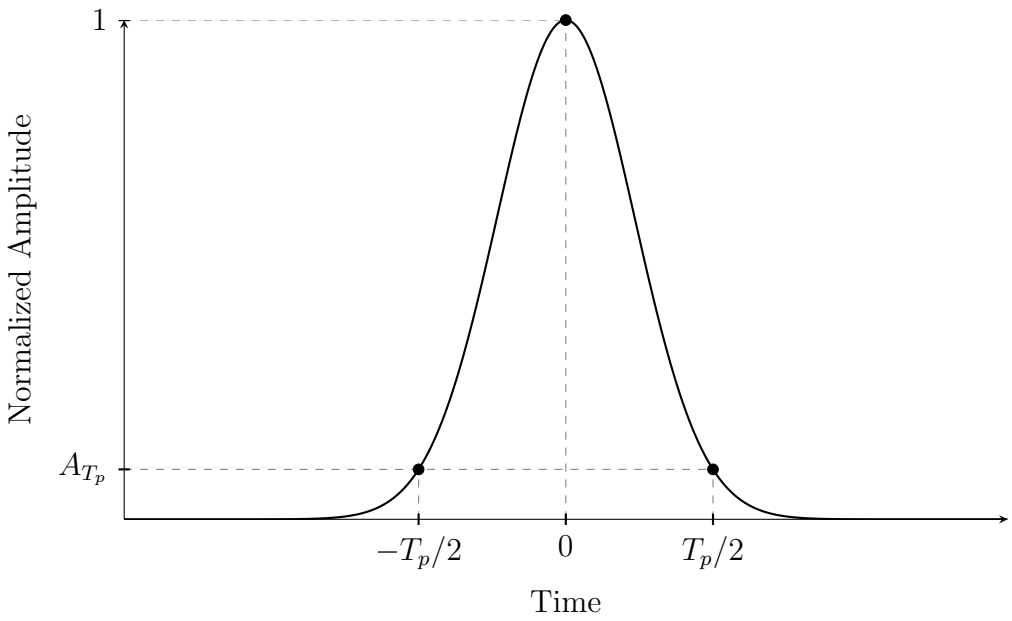

Figure 2.3: Definition of pulse width for a Gaussian pulse.

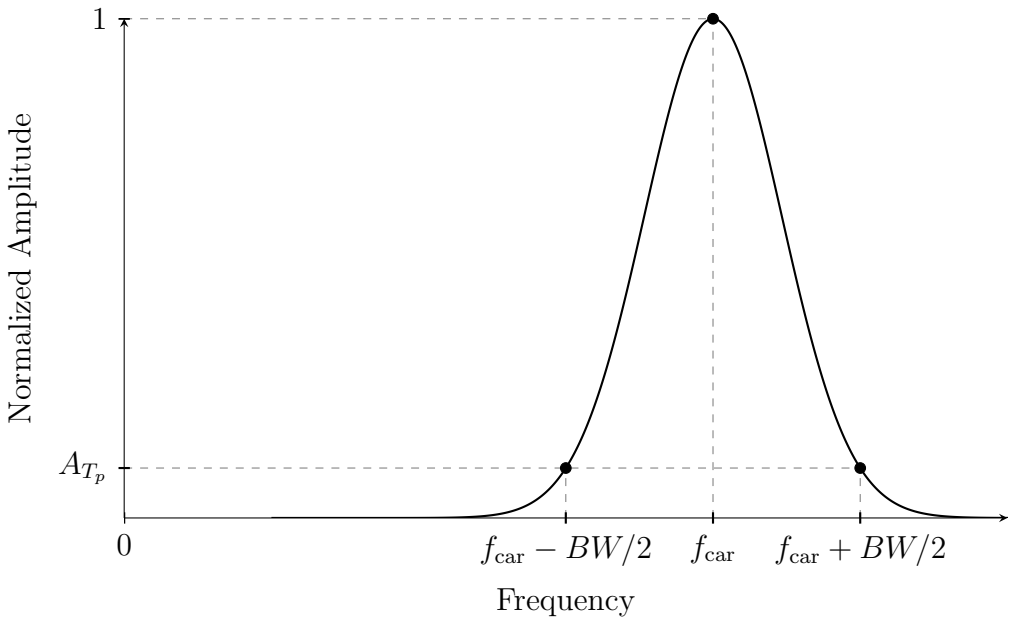

Figure 2.4: Definition of pulse bandwidth for a modulated Gaussian pulse.

2.4.2 Minimum Height

Presently in the literature many applications are limited to lossy dielectric materials where the attenuation is large enough that multiple reflections can be neglected [50, 51, 52, 32]. Otherwise, the impact of multiple reflections have been minimized by using broadband pulses with very fast rise times [38, 53]. Neither of these are suitable to the waveguide methods proposed in the following Chapter. The minimum height of the fluid that can be accurately measured has been defined in this Section in terms of the pulse width defined in Section 2.4.1. The pulse transmitted into the liquid is delayed by,

$$t_d = \frac{2h}{v_{\mathrm{g,Liq}}} \tag{2.18}$$

as a result of travelling twice the height of the liquid. At the minimum height the delay is equal to half the pulse duration of the signal [53],

$$t_d = \frac{T_p}{2} \tag{2.19}$$

This definition allows for the leading edge of the transmitted pulse to coincide with the peak of the reflected pulse. Substituting Equation 2.19 into Equation 2.18 and considering only the maximum group velocity in the liquid ($v_{\mathrm{g,Liq,Max}}$) gives the minimum height of the liquid,

$$h_{\min} = \frac{v_{\mathrm{g,Liq,Max}} T_p}{4} \tag{2.20}$$

For a TEM wave the group velocity is highest when $\epsilon_{\mathrm{r,Liq}} = 1$, which corresponds to $v_{\mathrm{g,Liq,Max}} = c$.

The total error introduced due to the overlap of all transmitted pulses can be derived from the series of infinite reflections [48]. The total received signal for an input signal $y(t)$ is,

$$y_r(t) = \Gamma_1 y(t) + T_{12}T_{21}\Gamma_3 y(t - t_d) + T_{12}T_{21}\Gamma_3^2\Gamma_2 y(t - 2t_d) + \cdots \tag{2.21}$$

which can be simplified to,

$$y_r(t) = \Gamma_1 y(t) + T_{12}T_{21}\Gamma_3 \sum_{n=0}^{\infty} \Gamma_2^n \Gamma_3^n y\left(t - (n+1)t_d\right) \tag{2.22}$$

Where,

$$T_{21} = 1 + \Gamma_1 \ , \ T_{12} = 1 + \Gamma_2 \ , \ \Gamma_2 = -\Gamma_1 \tag{2.23}$$

For a short circuit termination, $\Gamma_3 = -1$. Applying Equation 2.23, Equation 2.22 reduces to,

$$y_r(t) = \Gamma_1 y(t) + (\Gamma_1^2 - 1) \sum_{n=0}^{\infty} \Gamma_1^n y(t - (n+1)t_d) \tag{2.24}$$

Changing the index to $n = 1$ gives the simplified expression for the received pulse,

$$y_r(t) = \Gamma_1 y(t) + (\Gamma_1^2 - 1) \sum_{n=1}^{\infty} \Gamma_1^{n-1} y(t - nt_d) \tag{2.25}$$

The total reflection coefficient can be defined relative to $t = 0$ and using,

$$\Gamma_T \equiv \frac{y_r(0)}{y(0)} \tag{2.26}$$

utilizing the symmetry of the Gaussian pulse, $y(t) = y(-t)$,

$$\Gamma_T = \Gamma_1 + (\Gamma_1^2 - 1) \sum_{n=1}^{\infty} \Gamma_1^{n-1} y(nt_d) \tag{2.27}$$

The error introduced due to multiple reflections (Γ_{error}) can now be isolated,

$$\Gamma_T = \Gamma_1 + \Gamma_{\text{error}} \tag{2.28}$$

$$\Gamma_{\text{error}} = (\Gamma_1^2 - 1) \sum_{n=1}^{\infty} \Gamma_1^{n-1} y(nt_d) \tag{2.29}$$

For a Gaussian pulse, the quantity $y(nt_d)$ decreases exponentially.

$$y(nt_d) = \exp\left(\frac{-(nt_d)^2}{2\tau_0^2}\right) \tag{2.30}$$

Rearranging Equation 2.15 for τ_0 and substituting into Equation 2.30 gives,

$$y(nt_d) = \exp\left(\frac{-\left(\frac{nT_p}{2}\right)^2}{2\left(\frac{T_p}{\sqrt{-8\ln(A_{T_p})}}\right)^2}\right) \tag{2.31}$$

Which reduces to,

$$y(nt_d) = (A_{T_p})^{n^2} \tag{2.32}$$

$$\Gamma_{\text{error}} = (\Gamma_1^2 - 1)\sum_{n=1}^{\infty}\Gamma_1^{n-1}(A_{T_p})^{n^2} \tag{2.33}$$

A_{T_p} is significantly less than 1 by definition, therefore, the terms for $n > 1$ will not contribute significant error to measurements and can be neglected.

$$\Gamma_{\text{error}} \approx (\Gamma_1^2 - 1)A_{T_p} \tag{2.34}$$

The maximum absolute error introduced will occur when the reflection coefficient is small ($\Gamma_1 \approx 0$). The maximum absolute error introduced due to multiple reflections is,

$$|\Gamma_{\text{error,max}}| = A_{T_p} \tag{2.35}$$

The above derivation is only valid at $t = 0$. Where $t = 0$ is set to correspond to the peak amplitude of the first received signal. The error introduced adjacent to this time must be considered to ensure that the first reflected pulse is distinguishable. A range of values for A_{Tp} have been investigated in the following figures with $\Gamma_1 = 0.1$. At $A_{Tp} = 10^{-2}$ the first reflection is not distinguishable, as shown in Figure 2.5. When A_{Tp} is reduced to 10^{-3} the first pulse becomes distinguishable, however, the peak of the first reflected pulse is shifted slightly, refer to Figure 2.6. This peak shift would result in height measurement error. For $A_{Tp} \leq 10^{-4}$ the first reflected pulse is distinguishable and the error due to peak shifting is negligible. For reference, these figures are given in Figure 2.7 and Figure 2.8.

From Equation 2.17 the bandwidth of the signal is increased with decreasing A_{Tp}. Therefore, it is preferred to choose the highest value of A_{Tp} that will allow for the error introduced to be negligible. In this thesis, the value of $A_{Tp} = 10^{-4}$ has been used.

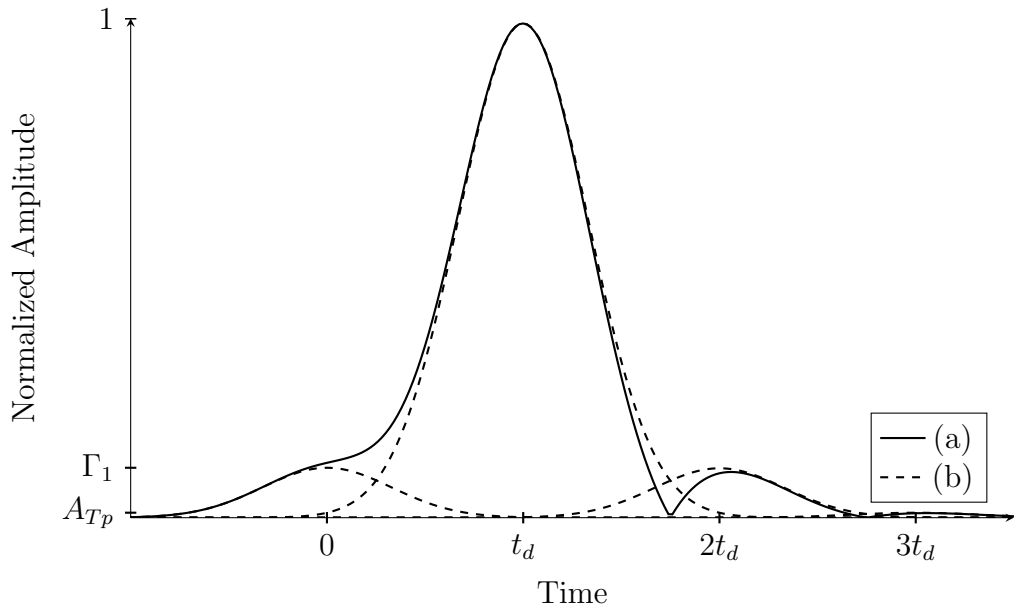

Figure 2.5: Envelope of the typical received time domain pulses as a result of multiple reflections for $A_{Tp} = 10^{-2}$. (a) Received signal and (b) individual reflections.

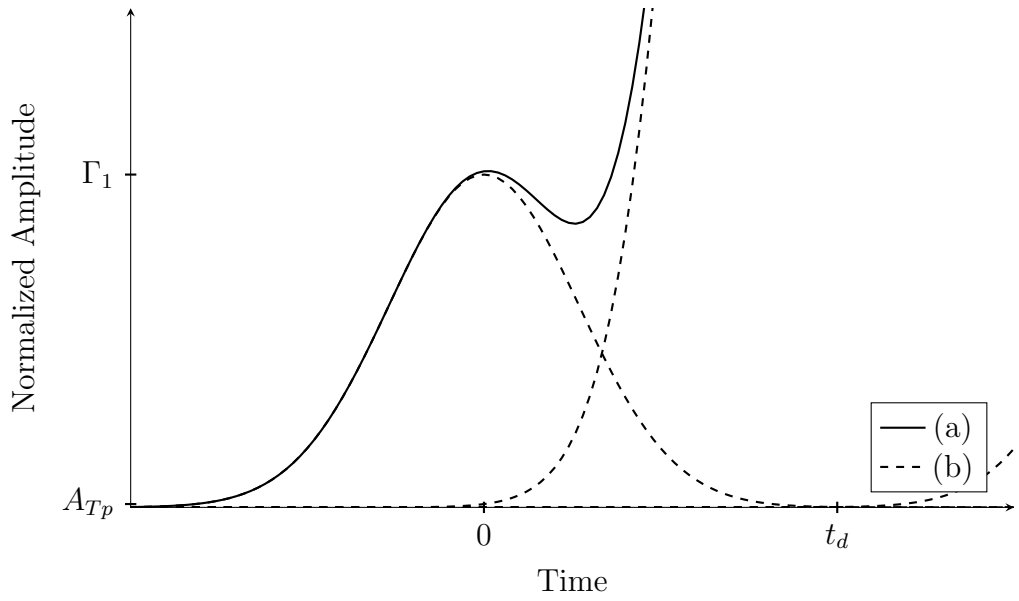

Figure 2.6: Envelope of the typical received time domain pulses as a result of multiple reflections for $A_{Tp} = 10^{-3}$. (a) Received signal and (b) individual reflections.

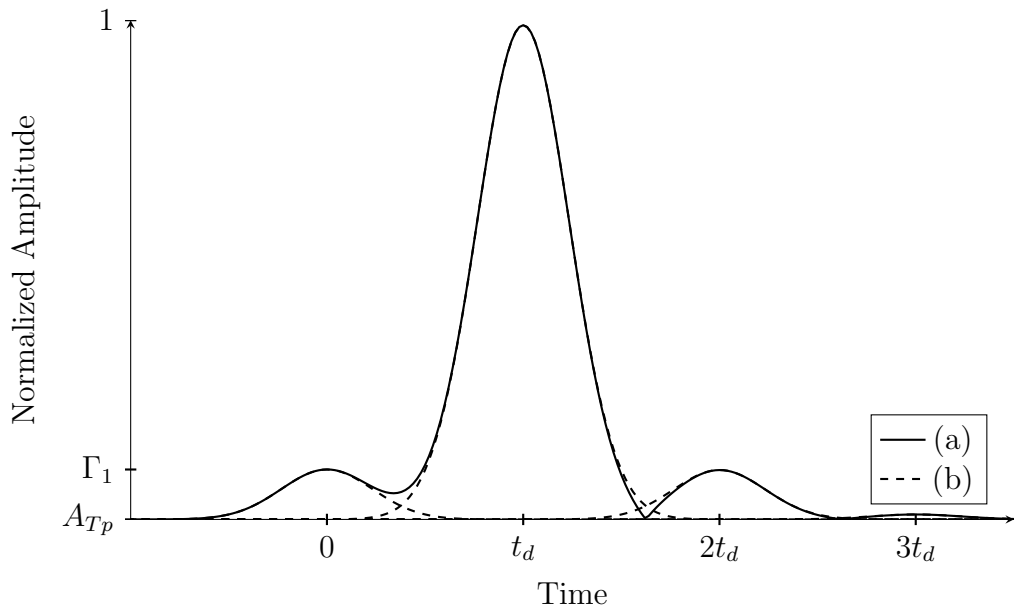

Figure 2.7: Envelope of the typical received time domain pulses as a result of multiple reflections for $A_{Tp} = 10^{-4}$. (a) Received signal and (b) individual reflections.

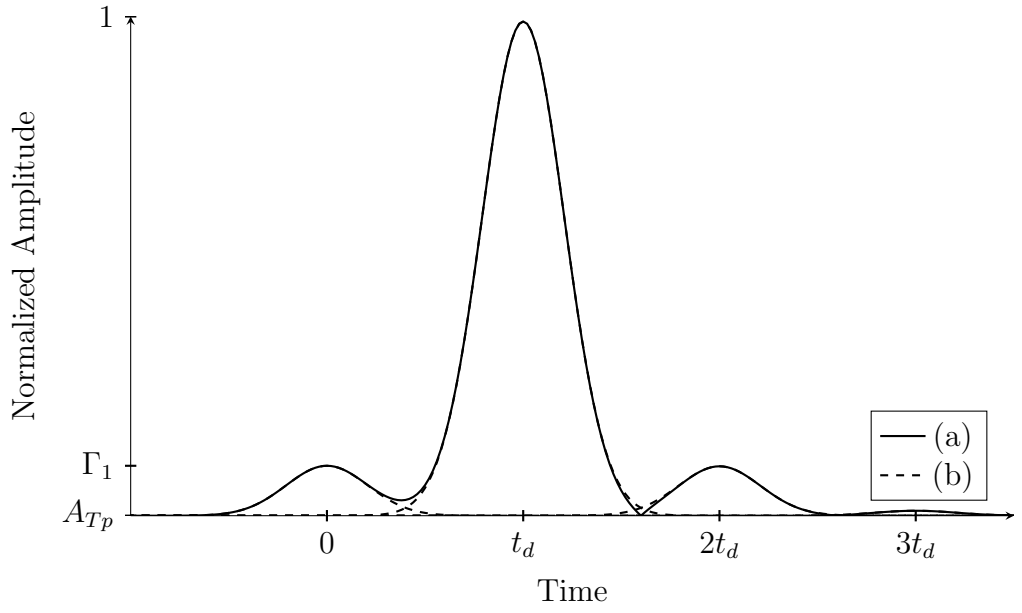

Figure 2.8: Envelope of the typical received time domain pulses as a result of multiple reflections for $A_{Tp} = 10^{-5}$. (a) Received signal and (b) individual reflections.

2.5 Summary

In this Chapter the proposed experimental setup, required background knowledge, and required definitions have been introduced. The basics of liquid permittivity and height measurement based on the peak amplitude and delay of the measured signal have been reviewed. For the case of a TEM wave, both the propagation velocity of a signal and the reflection coefficient were confirmed to be dependent only on the permittivity of the air and liquid. The concepts of pulse width and minimum height were defined. These are applicable to all time domain reflectometry applications, but will become of particular importance for the dispersive structure studied in the following Chapter. It was found that a pulse width definition (A_{Tp}) of 10^{-4} can be used to neglect the impact of multiple reflections.

Chapter 3

Analysis of Waveguides for TDR Applications

In order to use waveguides for time domain reflectometry applications, it is necessary to modify the fundamental concepts established in Chapter 2. The relevant background theory required will be briefly reviewed, including, probe configuration, the characteristic equation, waveguide modes and cut-off frequency. These topics are covered in Sections 3.1. The propagation and reflection properties of waveguides has been discussed in Section 3.2 and 3.4. The resulting impacts on the minimum height required will be discussed in Section 3.3. A detailed optimization strategy has been developed in Section 3.5 to determine the necessary probe parameters. This strategy provides the optimized probe dimensions, dielectric loading and pulse configuration for any particular application. Finally, measurement of the liquid permittivity and height necessitates accounting for the effects of dispersion on the received pulse. This is covered in Section 3.6. This thesis will focus on dielectric loaded circular waveguides, however the theory presented here could also be applied to other waveguides, such as rectangular, elliptical and coaxial.

3.1 Probe Configuration and Waveguide Theory

The proposed dielectric loaded circular waveguide is shown in Figure 3.1. The center of the waveguide core is loaded with a dielectric material of known permittivity ($\epsilon_{r,1} = \epsilon_{\mathrm{r,Load}}$) with a radius a. The circular waveguide wall of radius b is assumed to be a perfect electric conductor (PEC). The gap be-

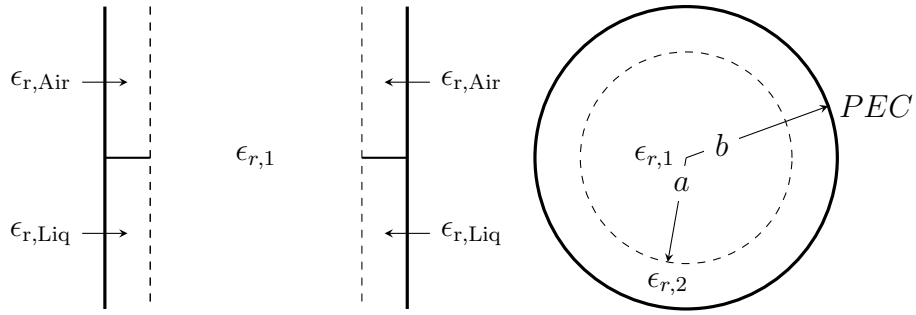

Figure 3.1: Side view (left) and cross section (right) of the dielectric loaded circular waveguide probe.

tween the dielectric loading and the conducting surface is filled with either air ($\epsilon_{r,2} = 1$) or the liquid under test ($\epsilon_{r,2} = \epsilon_{r,Liq}$).

The complex propagation constant (γ) is a frequency dependent parameter that determines the attenuation and propagation of the pulse. It is defined as [48],

$$\gamma = \alpha + j\beta \tag{3.1}$$

Where α is the attenuation constant and β is the phase constant. The propagation constant can be found by solving the characteristic equation [48],

$$F(\gamma) = 0 \tag{3.2}$$

The characteristic equation ($F(\gamma)$) is derived by solving Maxwell's equations subject to the boundary conditions. Maxwell's equations in source free region are [48],

$$\nabla \times \vec{E} = -j\omega\mu\vec{H} \tag{3.3}$$

$$\nabla \times \vec{H} = j\omega\epsilon\vec{E} \tag{3.4}$$

The boundary conditions that must be satisfied at the interface between the two dielectric filled regions are [54],

$$E_1^{\parallel} = E_2^{\parallel} \tag{3.5}$$

$$\epsilon_{r,1}E_1^{\perp} = \epsilon_{r,2}E_2^{\perp} \tag{3.6}$$

$$H_1^{\parallel} = H_2^{\parallel} \tag{3.7}$$

$$\mu_{r,1} H_1^{\perp} = \mu_{r,2} H_2^{\perp} \tag{3.8}$$

and the electric field on the surface of a perfect electric conductor must satisfy,

$$E_2^{\parallel} = 0 \tag{3.9}$$

Before the characteristic equation is presented, the concept of modes must first be introduced. A waveguide mode is a specific configuration of the electric and magnetic fields that allow the boundary conditions to be satisfied. For high frequencies, there will be multiple modes that are able to satisfy these conditions. These modes have distinct frequency dependent propagation and reflection properties. The three modes possible for a loaded circular waveguide are: transverse electric (TE), transverse magnetic (TM), and hybrid (HE). For TE modes the electric field is always perpendicular to the direction of propagation while for TM modes the magnetic field is always perpendicular to the direction of propagation. In other words, TE modes do not have an electric field component in the direction of propagation and TM modes do not have a magnetic field component in the direction of propagation. Hybrid modes have both electric and magnetic field components in the direction of propagation and are only supported by dielectric loaded waveguides [55].

The field configuration of each mode is indicated by the subscripts n and m. For a circular waveguide, n corresponds to the angular variation while m corresponds to the radial variation of the fields. For dielectric loaded waveguides, hybrid modes are generally required in order to satisfy all the boundary conditions, with the exception of TE_{0m} and TM_{0m} modes. TE_{0m} and TM_{0m} modes are able to satisfy the boundary conditions because the fields do not have angular dependence. Hybrid modes (HE_{nm}) require angular dependence, therefore $n \neq 0$ [56, 57].

Hybrid modes are highly complicated and the reflection coefficient cannot be calculated in terms of only the phase constant. For TM modes, the presence of the electric field in the direction of propagation results in the Brewster angle phenomenon that reduces the reflection coefficient to zero at some ge-

ometric and frequency dependent permittivity value [54]. Below and above this value there will exist multiple liquid permittivity values that will result in reflection coefficients of equal magnitude, which is not desired for permittivity measurement applications. TE_{0m} modes will be used in this thesis as the reflection properties can be modeled similar to TEM modes. Additionally, TE_{0m} modes are known to have the lowest conductor losses amongst available modes in homogeneously filled circular waveguides. A typical field pattern for the TE_{01} mode in a dielectric loaded circular waveguide is shown in Figure 3.2.

The full derivation of the characteristic equation is given in [58]. It can be found by using Equations 3.3 to 3.9 and setting $E_z = 0$,

$$\frac{J_1(x)}{xJ_0(x)} - \frac{J_1(y)N_1(zy) - J_1(zy)N_1(y)}{J_0(y)N_1(zy) - J_1(zy)N_0(y)}\frac{1}{y} = 0 \tag{3.10}$$

where,

$$x = k_1 a \ , \ y = k_2 a \ , \ z = b/a \tag{3.11}$$

$$k_1 = \sqrt{k_0^2 \epsilon_{r,1} + \gamma^2} \tag{3.12}$$

$$k_2 = \sqrt{k_0^2 \epsilon_{r,2} + \gamma^2} \tag{3.13}$$

$$k_0 = \frac{2\pi f}{c} \tag{3.14}$$

J_0 and J_1 are Bessel functions of the first kind of order 0 and 1 respectively. N_0 and N_1 are Bessel functions of the second kind of order 0 and 1 respectively. Equation 3.10 is a transcendental equation and therefore must be solved numerically. Either $\epsilon_{r,1}$ or $\epsilon_{r,2}$ may be complex valued to account for losses in the materials to give the resulting complex valued propagation constant γ. To simplify the solution process the losses in both materials have been neglected resulting in purely real values for $\epsilon_{r,1}$ and $\epsilon_{r,2}$ and allowing for the substitution of $\gamma^2 = -\beta^2$.

Figure 3.3 shows a typical dispersion relation for the TE_{0m} modes. A dispersion relation is used to describe the variation of the phase constant with respect to frequency. As discussed further in Section 3.2.3, non-linear variation

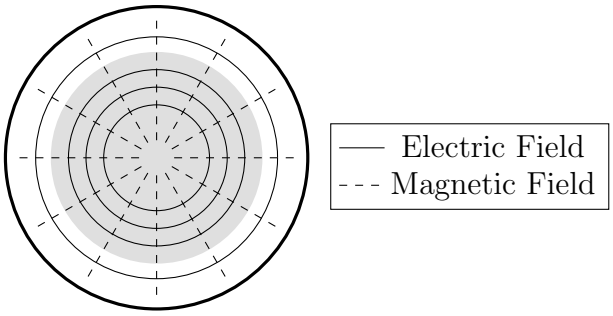

Figure 3.2: Field lines of the TE_{01} mode in the dielectric loaded circular waveguide.

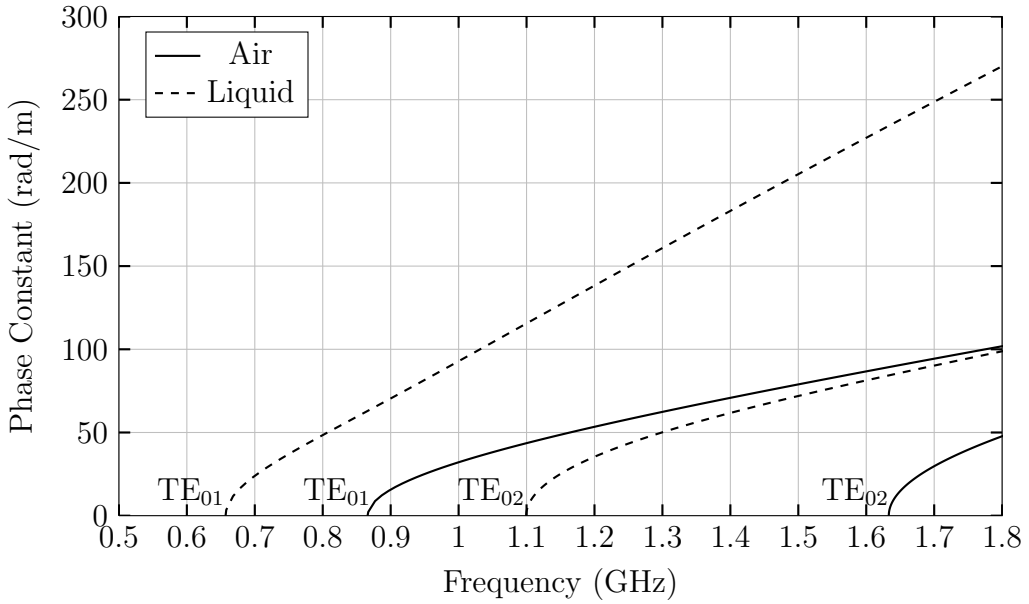

Figure 3.3: Dispersion relation for the TE_{01} and TE_{02} modes in air and with a liquid permittivity of 80. The probe has a permittivity loading of 9.74, inner radius 5.69cm and outer radius 6.90cm.

of β leads to dispersion of the signal. The cutoff frequency of a particular mode is defined as the frequency at which the phase constant equals to zero. A mode will not propagate below its cutoff frequency. A carrier frequency will be chosen such that it is operating above the cutoff frequency of the TE_{01} mode in the air filled region and below the cutoff frequency of the TE_{02} mode in the liquid filled region. This condition ensures monomode operation. In Figure 3.3, monomode operation is possible for frequencies between 0.866GHz and 1.10GHz.

3.2 Propagation

The propagation characteristics of a waveguide are frequency dependent and must be determined from the phase constant solution of the characteristic equation. The proximity of the carrier frequency of a signal to the cutoff of a particular mode will have a significant impact on the maximum group velocity in the liquid region and introduce dispersive effects. The ability to reduce the group velocity in the air region of the probe with dielectric loadings will allow for an increase in accuracy of height measurements.

3.2.1 Group Velocity

The speed of a pulse within a waveguide is determined by the group velocity [59]. The group velocity can be found from the phase constant [48],

$$v_g = \left(\frac{d\beta}{d\omega}\right)^{-1} \tag{3.15}$$

As discussed in Section 3.1, the phase constant is a frequency dependent property that varies with the geometry and the permittivity of the dielectrics within the probe. The group velocity in a waveguide is influenced by two factors: the proximity to the cutoff, and the permittivity of the dielectrics within the waveguide. At the cutoff frequency of a particular mode ($f_{c,0m}$) the group velocity is zero. When the operating frequency is much greater than the cutoff frequency the group velocity approaches to that of a TEM wave within the medium. The group velocity of a typical TE_{01} mode is given in Figure 3.4.

From Equation 2.20 the minimum height of the fluid is dependent on the peak group velocity within the liquid. This may not occur at $\epsilon_{r,Liq} = 1$ as is the case for a TEM probe. As stated previously, the group velocity is dependent on the proximity to cutoff and the permittivity of the materials within the probe. As the permittivity of the liquid within the probe is increased, the cutoff frequency of all modes will be decreased [60], which results in an increase in group velocity. However, the presence of the liquid results in a decrease in group velocity as it would for a TEM wave. The net result is dependent on the geometry and dielectric loading of the structure. A typical result is given in Figure 3.5.

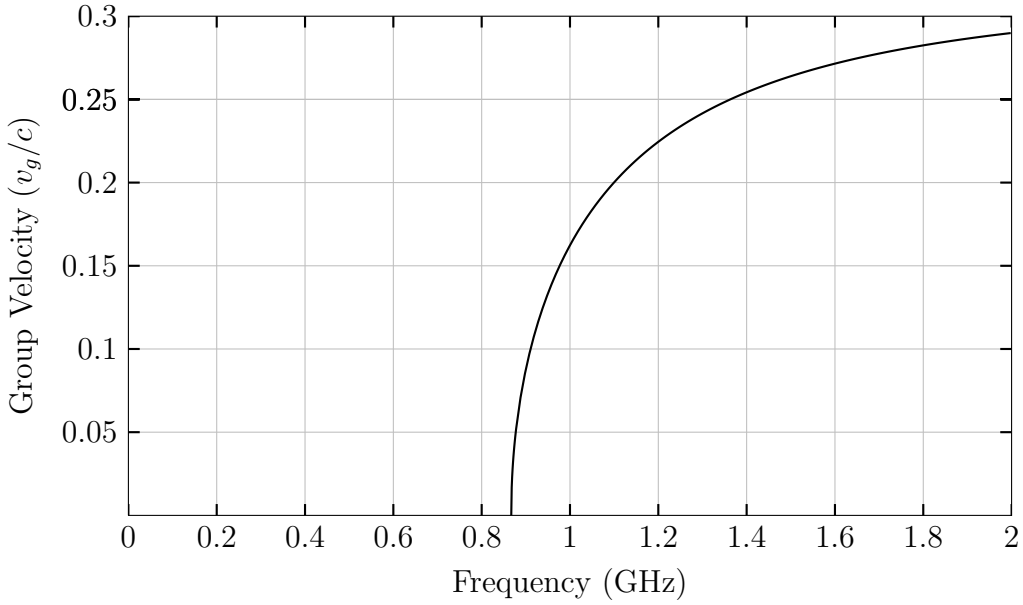

Figure 3.4: Group velocity of the TE_{01} mode in the air filled region of the probe with a permittivity loading of 9.74, inner radius 5.69cm and outer radius 6.90cm.

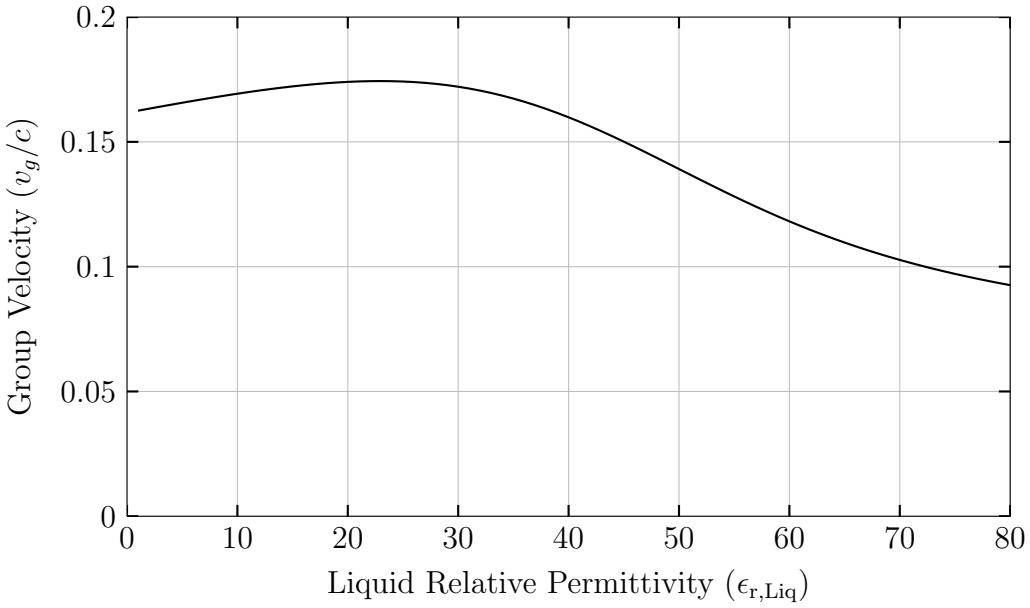

Figure 3.5: Group velocity of the TE_{01} mode in the liquid filled region of the probe with a permittivity loading of 9.74, carrier frequency of 1GHz, inner radius 5.69cm and outer radius 6.90cm.

3.2.2 Height Measurement Accuracy

The error in height measurement (∂h) due to error in the finite time measurement (∂t) can be derived from the group velocity of the signal in the air filled region of the probe. Rearranging Equation 2.3 and 2.4,

$$h = L - \frac{v_g t}{2} \tag{3.16}$$

taking the partial derivative with respect to time gives,

$$\partial h = -\frac{v_g \partial t}{2} \tag{3.17}$$

The accuracy improvement of height measurement (Δh) relative to a TEM probe ($v_g = c$) is defined as the ratio of the error introduced for the TEM and TE cases for a finite time measurement error ∂t,

$$\Delta h = \frac{-c\partial t/2}{-v_g \partial t/2} \tag{3.18}$$

which reduces to,

$$\Delta h = \frac{c}{v_g} \tag{3.19}$$

From the above equations it can be concluded that the error in height measurement varies linearly with the group velocity of the signal, allowing more accurate height measurements to be made by reducing the group velocity of the signal. Alternatively, if a minimum height error is required for a given application, the minimum time resolution of the accompanying measurement devices could be reduced by using slow wave structures.

3.2.3 Impacts of Dispersion on TDR

Dispersion occurs when the group velocity of the signal varies significantly over the frequency range of the signal. This variation causes different frequency components to travel at different velocities and leads to pulse spreading [61, 62]. Design strategies have been introduced in this thesis to utilize dispersive modes, which are not a typical issue with TEM probes. Dispersion theory used in fiber optic communication systems has been applied here [63]. In communication systems, dispersion must be limited to avoid the overlap of sequential pulses. The impacts of overlapping pulses will be discussed in detail

in Section 3.3.

A full derivation of pulse propagation in a dispersive media has been derived in Chapter 3 of [63]. The key results used in this thesis are presented here in Equations 3.20 to 3.25. In order to derive an analytical expression, the propagation constant is approximated as a second order Taylor series,

$$\beta(\omega) \approx \beta_0 + \beta_0'(\omega - \omega_0) + \frac{1}{2}\beta_0''(\omega - \omega_0)^2 \tag{3.20}$$

where,

$$\beta_0 = \beta(\omega_0) \quad \beta_0' = \left.\frac{\partial\beta}{\partial\omega}\right|_{\omega=\omega_0} \quad \beta_0'' = \left.\frac{\partial^2\beta}{\partial\omega^2}\right|_{\omega=\omega_0} \tag{3.21}$$

Where ω_0 is the center frequency of the pulse spectrum. In typical TDR applications, either a step or Gaussian pulse is used. Secant-squared pulses have a similar shape to the Gaussian pulse and have been shown to have a superior time bandwidth product [64]. A Gaussian pulse requires less bandwidth than a step pulse and is mathematically simpler than the secant-squared type. Although the secant-squared pulse may provide superior performance in dispersive applications, the Gaussian pulse has been chosen to allow for a mathematical solution while utilizing a standard TDR pulse configuration. The pulse has been modulated with a carrier signal (f_{car}) to allow the signal to operate in the desired frequency range. In the time and frequency domain the modulated Gaussian pulse is,

$$y(t) = \cos(2\pi f_{\text{car}} t)\exp\left(\frac{-t^2}{2\tau_0^2}\right) \tag{3.22}$$

$$Y(f) = \tau_0\sqrt{2\pi}\exp\left(\frac{-(2\pi(f - f_{\text{car}})\tau_0)^2}{2}\right) \tag{3.23}$$

Using the above Taylor approximation, the envelope of the received pulse has been shown to be,

$$y_r(d,t) = \left[\frac{\tau_0^4}{\tau_0^4 + (\beta_0''2d)^2}\right]^{1/4}\exp\left[-\frac{(t - \beta_0'2d)^2\tau_0^2}{2(\tau_0^4 + (\beta_0''2d)^2)}\right] \tag{3.24}$$

Where d is the distance traveled by the pulse. By inspection, the peak occurs at $t - \beta_0'2d = 0$ which is independent of the dispersive property β_0''. Therefore, for a second order approximation, dispersion does not shift the peak location of

the pulse. The second order approximation is valid for determining the probe parameters, however, peak shifting may occur due to third order and higher components. Significant errors may be introduced if these are not taken into account. This has been discussed in detail in Section 3.6. Similarly, a reduction in amplitude must be taken into account to calculate the permittivity.

For an unchirped pulse the Gaussian pulse width will spread from τ_0 to τ after traveling a distance $2d$,

$$\tau = \left[\tau_0^2 + \left(\frac{\beta_0'' 2d}{\tau_0}\right)^2\right]^{1/2} \tag{3.25}$$

An unchirped signal is a signal where the frequency is constant with respect to time.

The spectral distribution and second order approximation of β are shown in Figure 3.6 for a probe with a permittivity loading of 9.74. Refer to Table 3.2 for additional parameters.

The effects of dispersion can be reduced by using a chirped carrier signal [63]. If the leading edge of the signal has a lower frequency than the falling edge, the leading edge will travel slower than the falling edge. This will result in pulse compression for a short distance after which the pulse will again begin to spread. Therefore, if the distance the pulse is going to travel can be estimated, it is possible to minimize the impact of dispersion. However, dispersion compensation methods will result in another potential source of error and have not be included in the solution procedure. The dispersionless solution can be found by simply setting $\beta_0'' = 0$ to determine if dispersion compensation methods are necessary.

3.3 Minimum Height

The dispersive behaviour of waveguides must be accounted for to accurately determine the minimum height, as defined in Section 2.4.2. Dispersion results in an increase in pulse width which corresponds to an increase in minimum height. The amount of pulse spreading is proportional to the dispersive

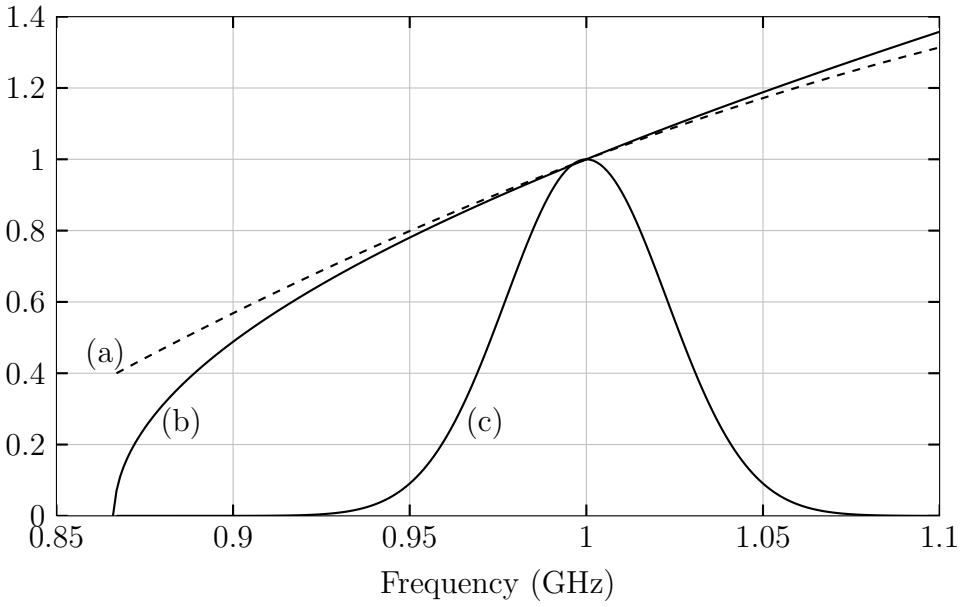

Figure 3.6: Normalized spectral comparison of (a) Taylor approximation of β, (b) β and (c) the modulated Gaussian pulse with a bandwidth of 196MHz. The outer radius of the probe is 6.90cm. The probe is loaded with a material that has a relative permittivity of 9.74 and radius of 5.69cm.

properties of the probe and the distance the pulse travels, as given by Equation 3.25. The substitution of τ in place of τ_0 in Equation 2.15 and revising Equation 2.20 gives,

$$h_{\min} = \frac{v_{\mathrm{g,Liq,Max}} \tau \sqrt{-8 \ln A_{Tp}}}{4} \tag{3.26}$$

Dispersion in the liquid can be neglected due to the reduction of cutoff frequency caused by the presence of the liquid. This reduction in cutoff frequency shifts the dispersion relation to the left, on the frequency scale, which allows the pulse to operate in a more linear region of the curve. Additionally, dispersion of the pulse in the liquid will not increase the minimum height as it will only cause further delay and reduced amplitude.

3.4 Reflection

The reflection at a lossless interface can be handled using the impedance method outlined in Section 2.3. Equation 2.5 can be rearranged in terms of only β for a TE wave at a lossless liquid. The impedance of the wave is given

by,

$$Z = \frac{E_x}{H_y} \tag{3.27}$$

For a TE wave, $E_z = 0$ and $H_z \neq 0$ [48],

$$E_x = \frac{-j\omega\mu}{k_c^2}\frac{\partial H_z}{\partial y} \tag{3.28}$$

$$H_y = \frac{-j\beta}{k_c^2}\frac{\partial H_z}{\partial y} \tag{3.29}$$

Then by Equation 3.27,

$$Z_{\mathrm{TE}} = \frac{\omega\mu}{\beta} \tag{3.30}$$

Substituting Equation 3.30 into Equation 2.5 and assuming $\mu = \mu_0$ gives,

$$\Gamma = \frac{\beta_1 - \beta_2}{\beta_1 + \beta_2} \tag{3.31}$$

Equation 3.31 is valid for frequencies less than the cutoff frequency of the TE_{02} mode in the liquid filled region of the probe. Above this frequency, energy is transferred into the higher order mode. This results in a sudden decrease in the reflection coefficient as shown in Figure 3.7. For this probe, below 1.1GHz, monomode operation is possible in both the air filled and liquid filled region up to a liquid permittivity of 80. Therefore, the maximum liquid permittivity considered for a particular application must be known ($\epsilon_{\mathrm{r,Max}}$). Operating in the monomode region of the liquid filled portion allows for the use of Equation 3.31, which has been shown to agree well with results from HFSS. Additionally, the high reflection coefficient in the monomode region allows for more accurate permittivity measurements to be made.

When losses are present ($\alpha \neq 0$), γ cannot be substituted for β as would be the case for the TEM reflection coefficient. That is,

$$\Gamma \neq \frac{\gamma_1 - \gamma_2}{\gamma_2 + \gamma_1} \tag{3.32}$$

The presence of losses allows the waveguide modes to satisfy the boundary conditions below the cutoff frequency of the lossless probe. This allows energy to be transferred into the higher order modes at the liquid discontinuity, as

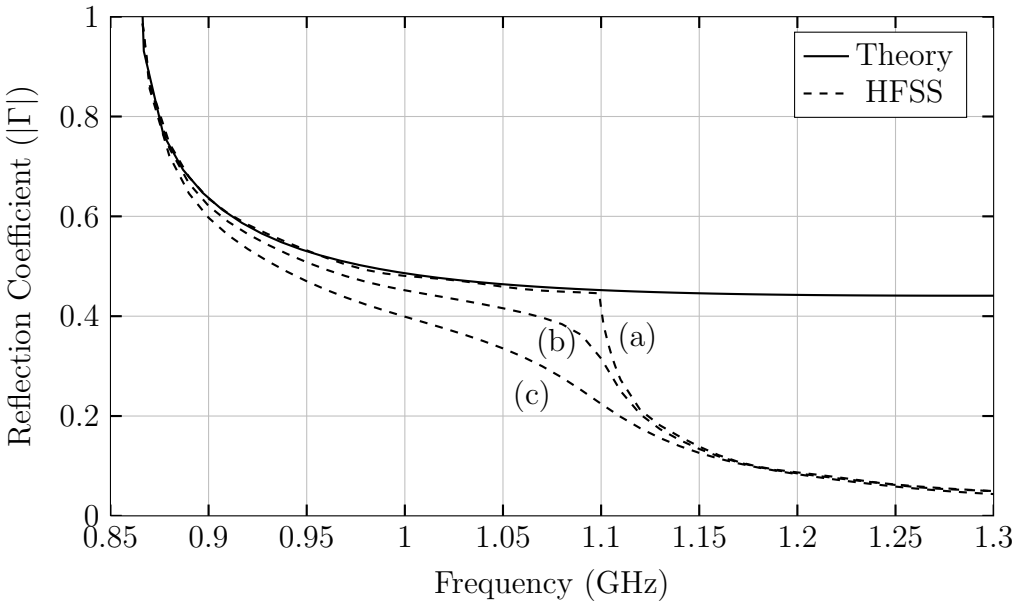

Figure 3.7: Comparison of the frequency dependent reflection coefficient using Equation 3.31 and as determined by HFSS for lossless and lossy liquids. The real component of the relative permittivity is 80. The liquids simulated in HFSS have a loss tangent of (a) $\tan\delta = 0$, (b) $\tan\delta = 0.05$ and (c) $\tan\delta = 0.2$. The dielectric loading has a relative permittivity of 9.74 and radius of 5.69cm. The outer radius of the probe is 6.90cm.

shown in Figure 3.7. Hence, monomode operation is not possible when losses are present. The portion of the signal transmitted into the higher order modes can be found using modal analysis [65].

Waveguide permittivity measurement applications typically require the thickness of the sample to be less than one-half of the guided wave length to suppress higher order modes [66]. Such a restriction is not practical for industrial applications where the liquid height may be large compared to the guided wavelength within the liquid filled region of the probe. These concepts will not be covered mathematically in this thesis due to the low loss assumption that has been made. However, the validity of this approximation has been studied for lossy liquids in Section 4.2.

The permittivity measurement accuracy of a probe is dependent on the variation of the reflection coefficient with respect to the relative permittivity of the liquid. The accuracy increase has been determined based on the ratio of the error in permittivity measurement for a TE and TEM probe. The error in the liquid permittivity measurement ($\partial\epsilon_{\mathrm{r,Liq}}$) due to a finite amplitude

measurement ($\partial\Gamma$) can be found by taking the partial derivative of Equations 3.31 for the TE probe, and 2.11 for the TEM probe. The increase in accuracy of permittivity measurement can be determined by finding the ratio of the error introduced for a TEM probe and TE probe. The permittivity accuracy increase is defined as,

$$\Delta\epsilon_r = \frac{\partial\Gamma_{\mathrm{TE}}/\partial\epsilon_r}{\partial\Gamma_{\mathrm{TEM}}/\partial\epsilon_r} \tag{3.33}$$

In other words, the accuracy of a TE probe will be greater than that of a TEM probe if the change of the reflection coefficient with respect to the liquid permittivity is greater than that of the TEM case.

3.5 Optimization Procedure

An iterative optimization procedure has been implemented using MATLAB to determine the probe dimensions (a, b), *c.f.* Figure 3.1, operating frequency range ($f_{c,01}$, $f_{c,02}$), dielectric loading ($\epsilon_{\mathrm{r,Load}}$), and probe performance parameters ($\Delta\epsilon_r$, Δh) for a desired probe length (L), minimum height (h_{min}), carrier frequency (f_{car}), pulse width definition (A_{Tp}), maximum liquid permittivity ($\epsilon_{\mathrm{r,Max}}$) and peak permittivity ($\epsilon_{\mathrm{r,Peak}}$). These terms have been defined previously, with the exception of peak permittivity. This parameter is necessary to optimize the probe design for a particular liquid application. The peak permittivity value is the permittivity at which the permittivity accuracy is optimized. This is used to determine the dielectric radius.

Normalized values for most probe parameters will be used to simplify the optimization procedure. The normalized values are defined for an outer radius of $b = 1$, with the exception of normalized carrier frequency. It has been shown that the outer radius can be determined based on the application defined properties which allows for computation of the remaining parameters. The absolute values can be defined in terms of b as follows,

$$a = a_n b \quad \beta = \frac{\beta_n}{b} \quad v_g{=}v_{g,n} \quad \beta_0'' = \beta_{0,n}'' b \quad \tau_0 = \tau_{0,n} b \quad f = \frac{f_n}{b} \tag{3.34}$$

Where f_n and f correspond to the normalized and absolute cutoff frequencies. Applying Equation 2.4, 3.26 and 3.34 to Equation 3.25 results in an equation for b in terms of the normalized values, dispersive properties of the probe,

length of the probe and the minimum height,

$$b = \frac{1}{\tau_{0,n}} \sqrt{\left(\frac{4h_{\min}}{v_{\mathrm{g,Liq,Max}} \sqrt{-8 \ln(A_{Tp})}} \right)^2 - \left(\frac{\beta''_{0,n} 2(L - h_{\min})}{\tau_{0,n}} \right)^2} \tag{3.35}$$

The parameters which determine b are dependent only on the normalized dielectric radius (a_n) and the chosen carrier frequency within the useable monomode frequency range. Monomode operation is ensured if the carrier frequency is above the normalized cutoff frequency of the TE_{01} mode in the air filled region ($f_{c,01,n}$) and below the normalized cutoff frequency of the TE_{02} mode in the liquid filled region ($f_{c,02,n}$). To simplify calculation requirements the normalized carrier frequency is defined relative to the monomode operating frequency range,

$$f_{\mathrm{car,n}} = \frac{f'_{\mathrm{car,n}} - f_{c,01,n}}{f_{c,02,n} - f_{c,01,n}} \tag{3.36}$$

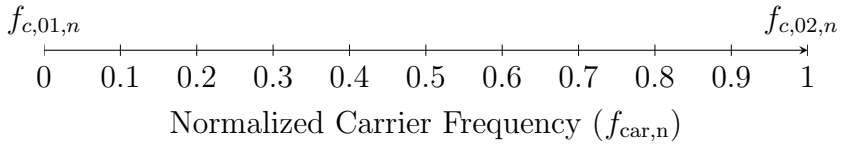

Figure 3.8: Definition of normalized carrier frequency.

Where $f'_{\mathrm{car,n}} = f_{\mathrm{car}}/b$ and the normalized carrier frequency satisfies $0 < f_{\mathrm{car,n}} < 1$. This allows for easy selection and comparison of the carrier frequency regardless of the monomode operating limits. Additionally, when $f_{\mathrm{car,n}} = 0.5$ the carrier signal is at the center of the useable monomode frequency range and allows for all available bandwidth to be used. The definition of normalized carrier frequency is illustrated in Figure 3.8. Values of $f_{\mathrm{car,n}} < 0.5$ would result in a reduced useable bandwidth while operating in the more dispersive region, therefore these values are not considered. As the normalized carrier frequency is increased, it approaches the upper limit of the frequency range. An increase in normalized carrier frequency results in a decrease in useable bandwidth. Thus, the normalized bandwidth used is defined as,

$$BW_n = 2(f_{c,02,n} - (f_{\mathrm{car,n}}(f_{c,02,n} - f_{c,01,n}) + f_{c,01,n})) \tag{3.37}$$

From Equation 2.17 it was shown that the Gaussian pulse width (τ_0) can be

determined based on the bandwidth of the signal. Additionally, the normalized Gaussian pulse width ($\tau_{0,n}$) was defined in Equation 3.34. Therefore, the normalized Gaussian pulse width is determined based on the normalized carrier frequency. As a result, b and all other resulting probe parameters can be compared and determined based on the same range of a_n and $f_{\text{car,n}}$. The normalized radius has been solved over then range of $0 < a_n < 1$ to a resolution of 0.001. The normalized carrier frequency has been solved over the range of $0.5 \leq f_{\text{car,n}} < 1$ to a resolution of 0.01. The performance of the probe is more sensitive to fluctuations in a_n, thus, it must be evaluated at a higher resolution than $f_{\text{car,n}}$.

To illustrate the variation of the key parameters discussed in this section, example figures have been provided for an application with requirements given in Table 3.1. A probe with a permittivity loading of 9.74 has been used. The parameters of this probe are summarized in Table 3.2. The permittivity loading of 9.74 was found after multiple iterations to satisfy the application specific requirements.

Table 3.1: Probe parameters for example Figures in Section 3.5.

Parameter	Value
$\epsilon_{\text{r,Peak}}$	60
$\epsilon_{\text{r,Max}}$	80
A_{Tp}	10^{-4}
L	3m
h_{min}	1m
f_{car}	1GHz

The first step is to determine the normalized cutoff frequency of the dominant mode in air and the first higher order mode in the liquid. Higher order modes will have a significant impact on the performance of the probe, therefore, it is important to take them into account when choosing the thickness of the dielectric loading. The presence of higher order modes can allow for energy to be transferred between modes due to imperfections in the waveguide construction or discontinuities [67]. This is referred to as modal dispersion, which is detrimental to the performance of the probe. Monomode operation can be ensured by choosing a_n only for values which result in $f_{c,02,n} > f_{c,01,n}$. A typical set of curves is given in Figure 3.9. The presence of the dielectric

loading reduces the rate at which the cutoff frequency in the liquid filled portion of the probe is decreased. This provides a range of monomode operation for high dielectric thicknesses.

In order to simplify the computational requirements, the phase constant has been solved for a limited range of values of a_n and $f_{\mathrm{car,n}}$. The values of normalized radius have been restricted to the range of $a_{\mathrm{n,min}} < a_n < 1$, where $a_{\mathrm{n,min}}$ is the smallest value that ensures $f_{c,02,n} > f_{c,01,n}$ and consequently monomode operation. The phase constant is first calculated in the air filled region to determine the dispersive properties (Equation 3.21), group velocity (Equation 3.15) and increase in height accuracy (Equation 3.19). The second order dispersive parameter is given in Figure 3.11. Next, the phase constant is calculated at the liquid permittivity where the peak accuracy is required. From the phase constant in air and the liquid filled regions of the probe, the reflection coefficient (Equation 3.31) and permittivity accuracy increase (Equation 3.33) can be calculated. A typical accuracy increase profile is given in Figure 3.10. For this application, it is shown that a normalized dielectric radius between 0.824 and 0.832 will result in the greatest increase in permittivity measurement accuracy.

The final component required to calculate the outer radius (b) is to determine the peak liquid group velocity. From Section 3.2.1 and Figure 3.5 it was shown that this value does not typically occur at $\epsilon_{\mathrm{r,Liq}} = 1$ as would be the case for a TEM probe. This necessitates solving for the phase constant at a range of liquid permittivity values to determine the permittivity where the group velocity is highest. The group velocity is calculated for the range of carrier frequencies but it is only necessary to calculate at the normalized radius where the accuracy is highest, in this case $0.824 \leq a_n \leq 0.832$. This allows for a significant reduction in the computational requirements. The peak group velocity and its corresponding liquid permittivity varies as shown in Figure 3.12.

Now the outer radius can be calculated over the range of normalized carrier frequencies using Equation 3.35. At lower values of normalized carrier frequency dispersive effects are dominant. This has been illustrated in Figure 3.15, where b has been solved with and without dispersion. For the dispersionless case, the outer radius decreases monotonically with increasing normalized

carrier frequency. For the dispersive case, the outer radius is highly dependent on the normalized carrier frequency. At high normalized carrier frequencies, the dispersive parameter $\beta''_{0,n}$ and the useable bandwidth are low (See Figure 3.11 and 3.13). These two effects result in dispersion being negligible for high normalized carrier frequencies. Dispersion and bandwidth are greatest at low normalized carrier frequencies. High bandwidth corresponds to a smaller time domain pulse, while dispersion corresponds to pulse spreading. These two competing effects necessitate a decrease in the outer radius at low normalized carrier frequencies to increase the absolute bandwidth and consequently satisfy the minimum height requirement. This is further illustrated in Figure 3.16 which shows the operating frequency range, carrier frequency and bandwidth for both the dispersive and non-dispersive cases.

The impact of losses can be reduced by operating the probe at low frequencies. The operating frequency can be controlled to some extent by choosing the normalized carrier frequency and dielectric loading. The normalized carrier frequency that provides the lowest higher order mode cutoff frequency is chosen. For the example figures provided, the trade-off between bandwidth and dispersion corresponds to a normalized carrier frequency of 0.58 and gives the desired carrier frequency of 1GHz. Note that several iterations are required in order to determine the permittivity loading which results in the desired carrier frequency, if possible.

All probe parameters are now known for a particular permittivity loading at a desired minimum height. If a lower frequency is desired, the permittivity of the loading can be increased. However, since dispersion increases faster than the rate of frequency reduction, there is a limit to the minimum possible operating frequency. This has been shown in the following Chapter. If a higher frequency is desired, the permittivity of the loading can be decreased. If the operating frequency is desired to be increased beyond the value given at a permittivity loading of one, then either the minimum height can be reduced or the probe length can be increased.

The results of the iterative procedure to obtain the required permittivity loading of 9.74 are given in Table 3.2. An initial guess with a permittivity loading of 5 is used. The result gives a carrier frequency of 1.561GHz. This

value is greater than the desired carrier frequency of 1GHz, therefore the permittivity loading is increased by 2 and the next value determined, otherwise the loading would be decreased by 2. The results with a permittivity loading of 1 and 3 have been included for comparison. The carrier frequency at a permittivity loading of 7 is found to be 1.243GHz. The next permittivity loading is determined using linear interpolation with the previous two values. This procedure is continued until the resulting carrier frequency is found to within the desired value to within ±5MHz, or until it is determined that a suitable permittivity value cannot be found.

In practice, materials with the desired permittivity loading may not be available. Probe parameters have been solved for permittivity loadings within ±1 of the desired permittivity loading. The results have been summarized in Table 3.3. It has been found that a small change in the desired permittivity does not have a significant impact on the performance properties of the probe, provided that the desired permittivity loading is not close to 1. The increase in accuracy of permittivity measurements varies by 0.2 while the increase in accuracy of height measurements varies by up to 0.3. Additionally, the carrier frequency varies by up to 71MHz.

Filling the probe with a dielectric loading has two important impacts on the cutoff frequency. When the loading is greater than 1, the wavelength at a particular frequency is increased, allowing for lower frequencies to satisfy the boundary conditions and therefore lowering the cutoff frequency. By the same reasoning, when the probe is filled with liquid, the cutoff frequency of the higher order modes will reduce rapidly. Finally, the amount of physical space available for the liquid to occupy is reduced, thereby lowering the rate at which the cutoff frequency of higher order modes is reduced.

Figure 3.14 shows the height measurement accuracy as the normalized carrier frequency increases. The permittivity accuracy is primarily dependent on the radius of the dielectric loading, and therefore, does not vary significantly with the normalized carrier frequency. The reflection coefficient and the increase in accuracy over the range of liquid permittivity values will be covered in Section 4.1.

Table 3.2: Example results of the iterative optimization procedure for the determiniation of dielectric loading, subject to the restraints given in Table 3.1.

f_{car} (GHz)	$\epsilon_{\mathrm{r,Load}}$	a_n	b (cm)	$f_{\mathrm{car,n}}$	$f_{c,01}$ (GHz)	$f_{c,02}$ (GHz)	$\frac{v_{\mathrm{g,Liq}}}{c}$	$\beta''_{0,n}$ ($\times 10^{-18}$)	$\frac{\lvert\Gamma_{\mathrm{TE}}\rvert}{\lvert\Gamma_{\mathrm{TEM}}\rvert}$	Δh	$\Delta\epsilon_r$
4.951	1.00	0.949	3.98	0.61	4.598	5.176	0.402	-46	0.59	2.7	11.7
2.241	3.00	0.909	5.23	0.59	2.022	2.393	0.266	-80	0.54	4.0	7.2
1.561	5.00	0.880	5.95	0.59	1.384	1.685	0.222	-100	0.51	4.8	5.8
1.243	7.00	0.855	6.43	0.59	1.087	1.351	0.197	-116	0.48	5.4	5.0
1.090	8.53	0.838	6.73	0.59	0.945	1.191	0.184	-127	0.47	5.8	4.6
1.024	9.42	0.828	6.86	0.59	0.884	1.120	0.178	-133	0.46	6.0	4.4
1.002	9.74	0.824	6.90	0.58	0.866	1.100	0.175	-139	0.46	6.1	4.3

Table 3.3: Variation of the probe parameters within ± 1 of the desired permittivity loading of 9.74.

f_{car} (GHz)	$\epsilon_{\mathrm{r,Load}}$	a_n	b (cm)	$f_{\mathrm{car,n}}$	$f_{c,01}$ (GHz)	$f_{c,02}$ (GHz)	$\frac{v_{\mathrm{g,Liq}}}{c}$	$\beta''_{0,n}$ ($\times 10^{-18}$)	$\frac{\lvert\Gamma_{\mathrm{TE}}\rvert}{\lvert\Gamma_{\mathrm{TEM}}\rvert}$	Δh	$\Delta\epsilon_r$
1.073	8.74	0.835	6.75	0.58	0.932	1.175	0.181	-132	0.47	5.9	4.5
1.038	9.24	0.829	6.81	0.58	0.900	1.138	0.178	-136	0.47	6.0	4.4
1.017	9.49	0.827	6.87	0.58	0.881	1.116	0.176	-137	0.46	6.1	4.4
1.002	9.74	0.824	6.90	0.58	0.866	1.100	0.175	-139	0.46	6.1	4.3
0.987	9.99	0.821	6.93	0.58	0.853	1.084	0.173	-141	0.46	6.2	4.3
0.970	10.24	0.819	6.98	0.58	0.837	1.066	0.172	-142	0.46	6.3	4.2
0.944	10.74	0.813	7.02	0.58	0.813	1.038	0.169	-146	0.46	6.4	4.1

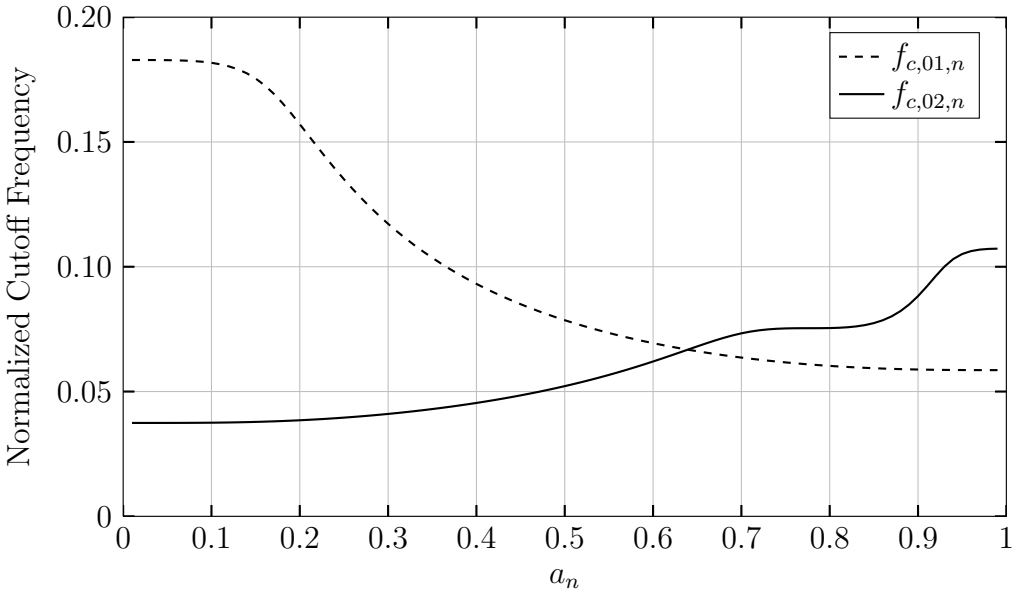

Figure 3.9: Normalized cutoff frequency for the dominant mode in air ($f_{c,01,n}$) and the first higher order mode ($f_{c,02,n}$) at the maximum liquid permittivity ($\epsilon_{\mathrm{r,Max}}$) for all possible values of normalized dielectric radius (a_n).

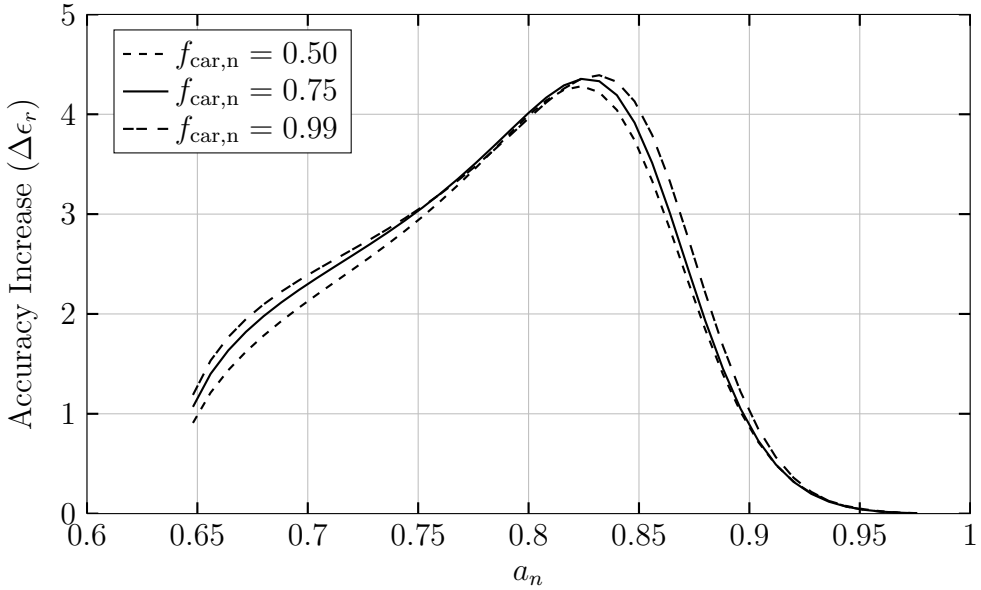

Figure 3.10: Permittivity accuracy increase over the range of normalized dielectric radius at a normalized carrier frequency of 0.50, 0.75 and 0.99. Accuracy increase is reported relative to a TEM probe.

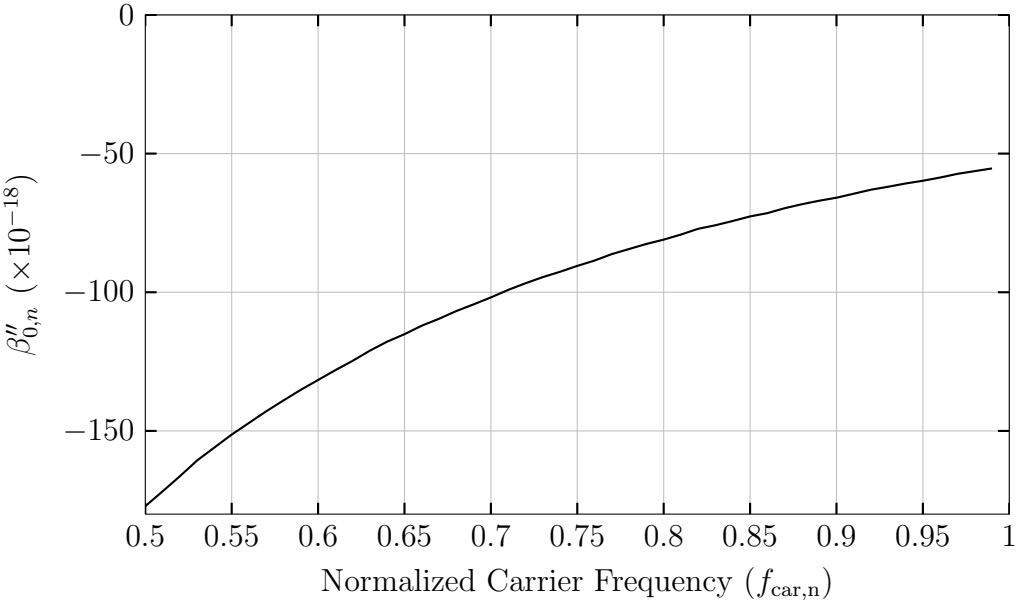

Figure 3.11: Dispersive behaviour over the range of normalized carrier frequencies. Solved at the normalized radius corresponding to the peak permittivity accuracy.

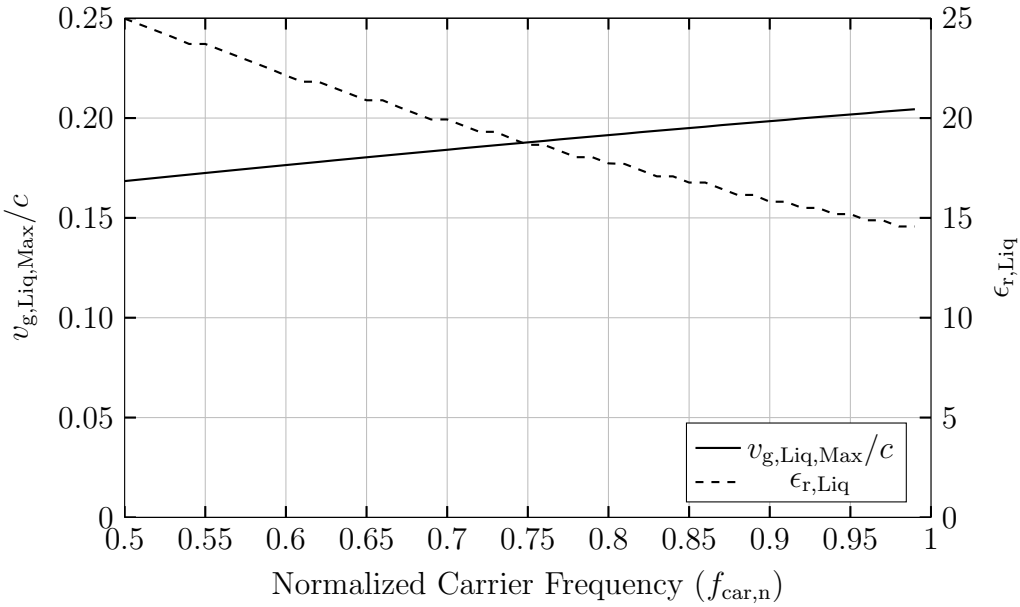

Figure 3.12: Peak liquid group velocity and the corresponding liquid permittivity where it occurs. Solved at the normalized radius corresponding to the peak permittivity accuracy.

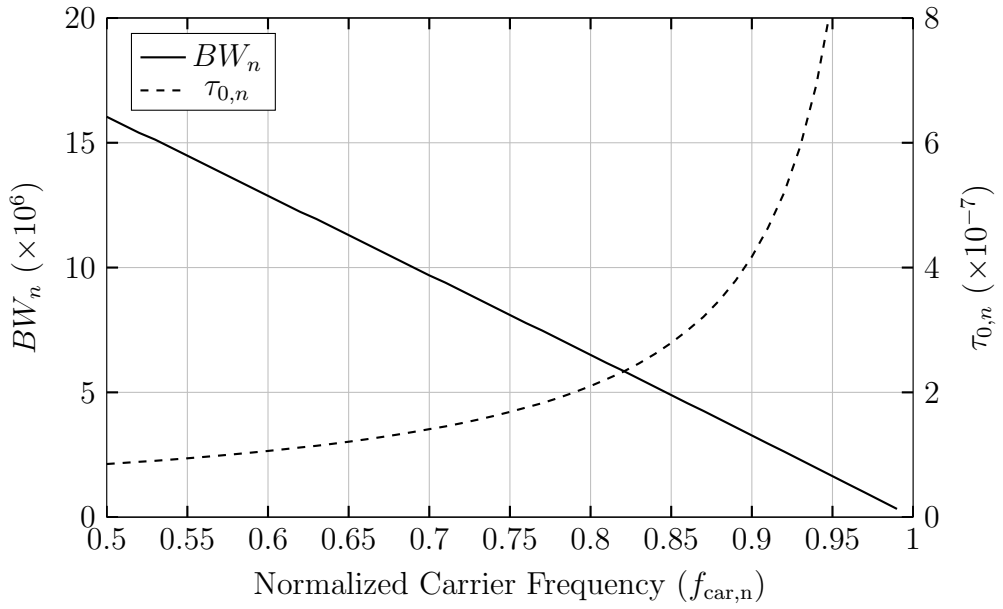

Figure 3.13: Normalized bandwidth and normalized Gaussian pulse width over the range of normalized carrier frequencies.

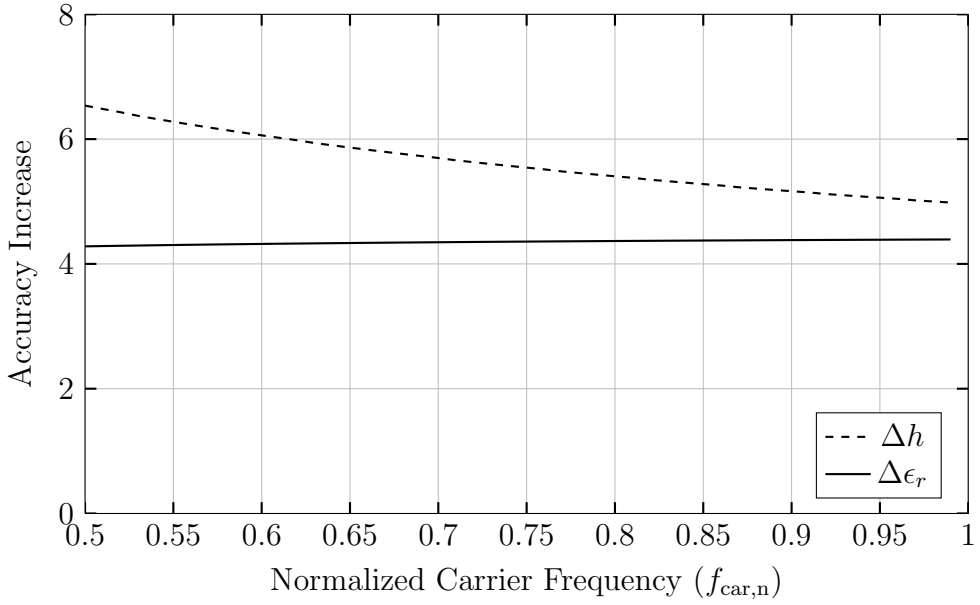

Figure 3.14: Permittivity and height accuracy increase over the range of normalized carrier frequencies. Solved at the normalized radius corresponding to the peak permittivity accuracy.

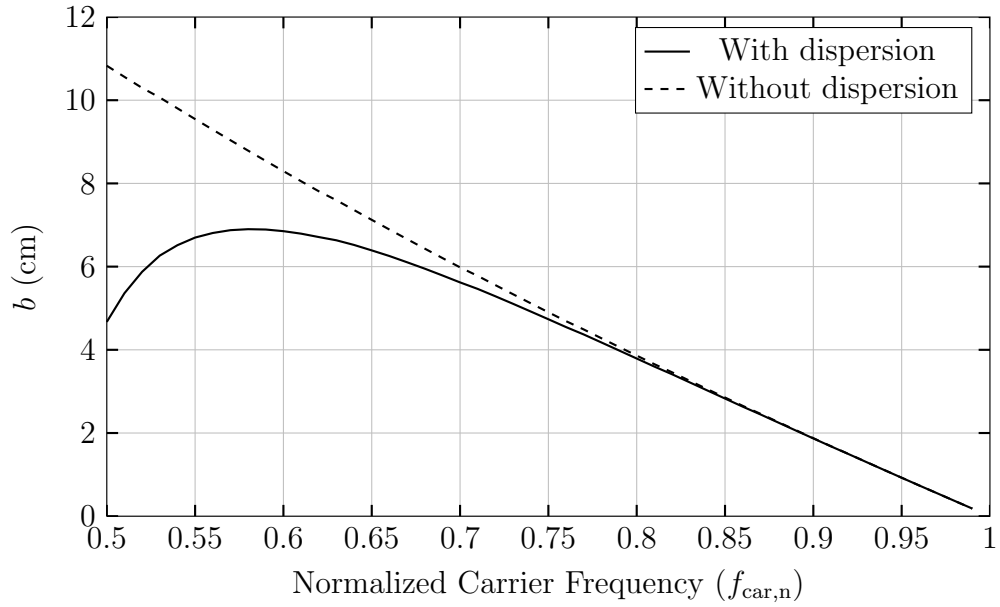

Figure 3.15: Outer probe radius over the range of normalized carrier frequencies, with and without dispersion. Solved at the normalized radius corresponding to the peak permittivity accuracy.

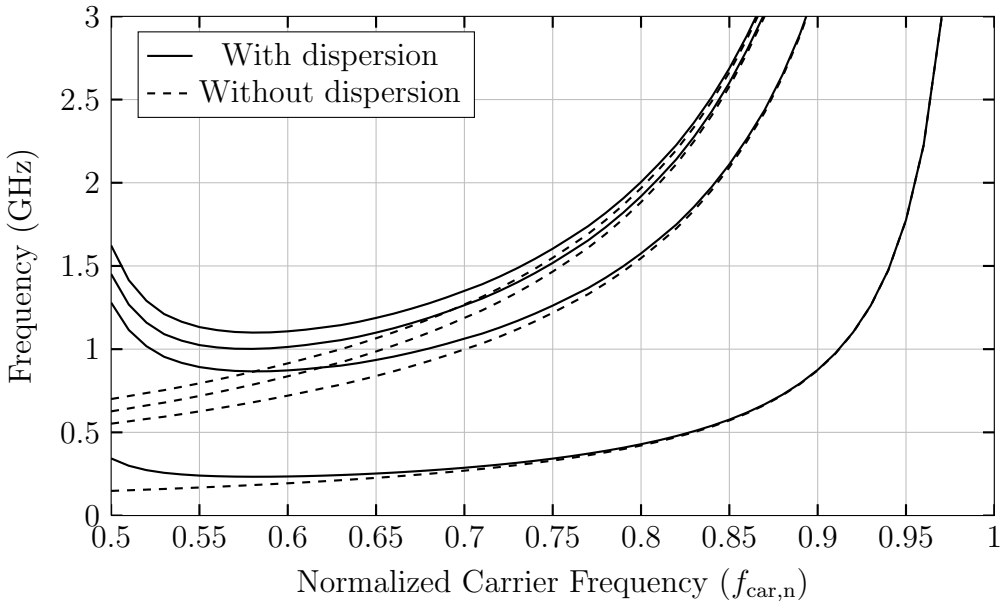

Figure 3.16: Cutoff frequency of higher order and dominant modes, carrier frequency and bandwidth over the range of normalized carrier frequencies. For each set, from top to bottom: $f_{c,02}$, f_{car}, $f_{c,01}$ and BW. Solved at the normalized radius corresponding to the peak permittivity accuracy.

3.6 Determining Height and Permittivity Values

As discussed in the preceding sections, the liquid permittivity and height can be determined from the amplitude and delay of the received signal. However, the effects of dispersion must first be accounted for. As discussed in Section 3.2.3 the second order approximation is useful for determining probe parameters but is not sufficient for measurement purposes. Third order effects have been shown to shift the peak of the pulse [68], which will introduce height measurement error. Equation 2.1 for a dispersionless signal has been modified to,

$$y_r(t) = \Gamma' y(t - t_1') \tag{3.38}$$

Where,

$$\Gamma' = \Gamma(A_{\text{disp}} + \Gamma_{\text{disp}}) \tag{3.39}$$

$$t_1' = t_1 + t_{\text{disp}} \tag{3.40}$$

Γ' is the measured reflection coefficient and t_1' is the measured delay. Γ is proportional to the liquid permittivity as determined by Equation 3.31. t_1 is proportional to the liquid height as determined by Equation 3.16. A_{disp} is defined as the peak amplitude of a dispersed pulse by taking the magnitude of Equation 3.24,

$$A_{\text{disp}} = \left[\frac{\tau_0^4}{\tau_0^4 + (\beta_0'' 2d)^2}\right]^{1/4} \tag{3.41}$$

The remaining parameters, Γ_{disp} and t_{disp} are proportional to the third order and higher dispersive properties of the probe and the distance the pulse travels. The total impact of dispersion can be found using the inverse Fourier transform,

$$y_p(d,t) = \mathcal{F}^{-1}\{Y(f)e^{-j\beta 2d}\} \tag{3.42}$$

Where $\mathcal{F}^{-1}\{\}$ is the inverse Fourier transform and $Y(f)$ is the Fourier transform of the input signal. The peak amplitude and peak delay have been solved numerically from Equation 3.42 to determine Γ_{disp} and t_{disp}. The results are given in Figure 3.18 and 3.19 for a probe with a permittivity loading of 9.74 and other parameters as described in Table 3.2. At the maximum expected pulse propagation distance of 4m the peak of the pulse is delayed by an addi-

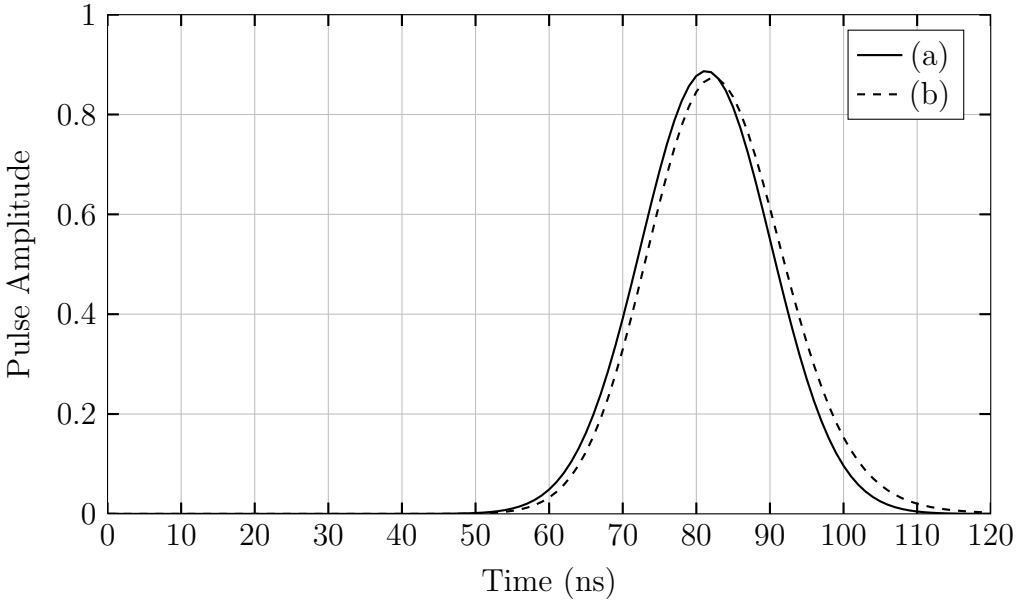

Figure 3.17: Dispersive effects on a pulse after traveling 4m, relative to an input pulse with an amplitude equal to 1. Calculated using (a) the second order Taylor approximation and (b) the Fourier method. The probe used has a permittivity loading of 9.74 with properties given in Table 3.2.

tional 0.96ns and the amplitude is further reduced by 0.0136. This is further illustrated by Figure 3.17, which shows the predicted pulse propagation and spreading due to the second order Taylor approximation and the result using the Fourier method. Using the Fourier method, the peak value occurs at 82.29ns, with an amplitude of 0.8737. Using the second order Taylor approximation the peak value occurs at 81.33ns, with an amplitude of 0.8873. This results in a maximum percent error of 1.16% and 1.56% for the delay and amplitude respectively. Such error is significant for measurement applications and should be accounted for.

Equation 3.42 has been modified to include the reflection at the liquid to give the received pulse,

$$y_r(d,t) = \mathcal{F}^{-1}\{\Gamma Y(f) e^{-j\beta 2d}\} \tag{3.43}$$

A lookup table can be generated by solving Equation 3.43 for the peak amplitude and peak delay over the range of expected liquid permittivity values and propagation distances. This lookup table can then be used to provide the one to one mapping necessary to determine the liquid permittivity and height

from the measured peak amplitude and peak delay.

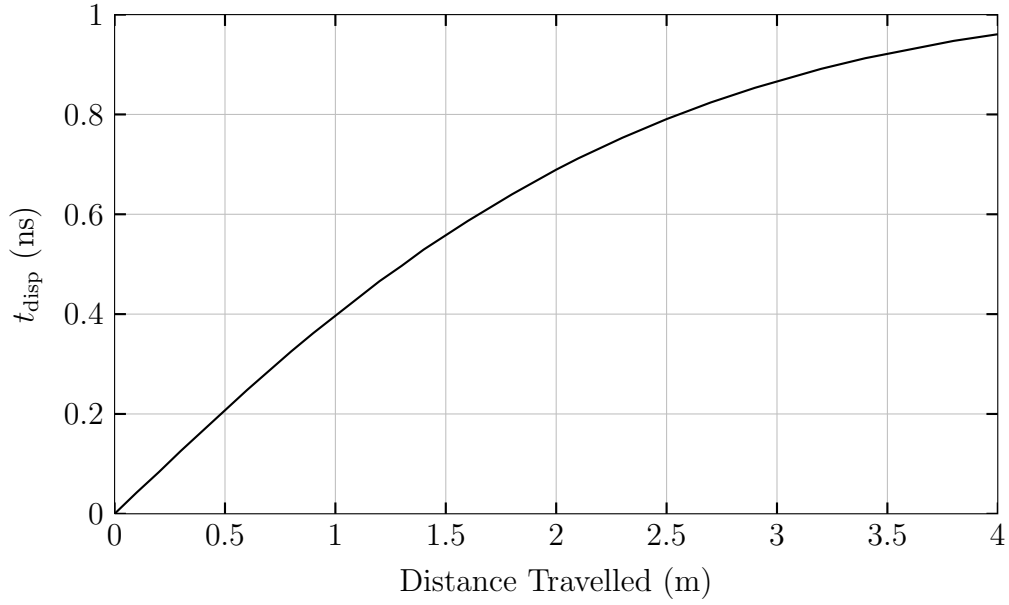

Figure 3.18: Time delay adjustment factor for a probe with a permittivity loading of 9.74 with properties given in Table 3.2.

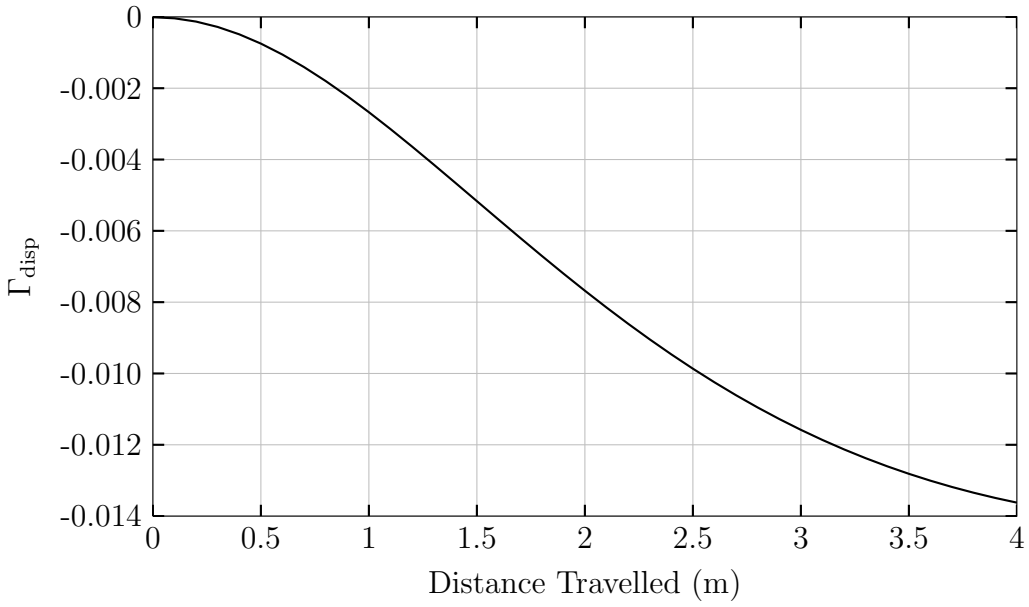

Figure 3.19: Reflection coefficient adjustment factor for a probe with a permittivity loading of 9.74 with properties given in Table 3.2.

Chapter 4

Performance Analysis

In this Section, the optimization procedure developed in Section 3.5 has been used to determine the probe parameters for a wide range of applications. The results have been confirmed with the simulation software, Ansoft HFSS. The design parameters and probe performance have been studied for lossy solutions of ethanol-water and acetic acid to determine the validity of the lossless approximation. It has been found that the design parameters determined using the lossless method can provide increased fluid height and characterization measurement accuracy for lossy applications at low frequencies.

4.1 High Permittivity Measurements of Lossless Liquids

The strategy outlined in Section 3.5 will be applied here to three applications involving high permittivity solutions and a range of minimum height values. The maximum permittivity of the liquids considered are 80, 60 and 45. The permittivity at which the accuracy is desired to be optimized is chosen to be at 75% of the maximum permittivity, corresponding to permittivities of 60, 45 and 30. These three applications are intended to illustrate the potential of TE waveguide probes for high permittivity liquids. Examples of high permittivity liquids include solutions that contain large amounts of water (80.1), glycerol (46.5), ethylene glycol (41.4), methanol (33.0) or ethanol (25.3). The number in parathensis is the static permittivity of the liquid [69].

To minimize the impact of liquid losses on the lossless method used, a carrier frequency of 1GHz has been chosen. A pulse bandwidth definition of

$A_{Tp} = 10^{-4}$ has been assumed. For all cases, a total probe length of 3m has been used based on the typical probe length for an industrial application [42]. Typical applications include large storage or mixing tanks. The permittivity loadings required in order to meet a range of minimum heights has been determined down to 1m.

To confirm the validity of the characteristic equation for lossless applications, the example probe used in Section 3.5 has been simulated using Ansoft HFSS for a range of frequencies and liquid permittivity values. The results are presented in Figures 4.1 and 4.2. The results shown for both the phase constant and reflection coefficient agree very well with the values predicted using the characteristic equation and the impedance based reflection coefficient equation.

The accuracy increase over the range of liquid permittivities for the example probe is given in Figure 4.3. The probe is shown to provide an increase in accuracy for any liquids with a relative permittivity greater than 25. Note that the accuracy results have been reported in multiples of TEM. For example, at the liquid permittivity at which the probe is optimized ($\epsilon_{\mathrm{r,Peak}} = 60$) the permittivity accuracy of the probe is 4.3 times that of a TEM probe. In other words, if a TEM probe can determine the relative permittivity to within ± 1 then the TE probe would have an accuracy of ± 0.23. It has also been observed that the greatest increase in permittivity accuracy may not occur at the permittivity at which the probe is optimized. The optimization procedure determines the radius of the dielectric loading that results in the greatest increase in permittivity accuracy at the desired liquid permittivity ($\epsilon_{\mathrm{r,Peak}}$). The greatest increase in permittivity accuracy over the range of liquid permittivities considered in this example occurs for a liquid with relative permittivity of approximately 75, corresponding to an increase in permittivity accuracy of 4.7 times that of a TEM probe.

For the three scenarios studied in Tables 4.1, 4.2 and 4.3 the trends between the various probe parameters are consistent. The most notable difference is that higher accuracy increases are possible at higher liquid permittivity values. This is largely due to the low variance of the TEM reflection coefficient at high permittivity values.

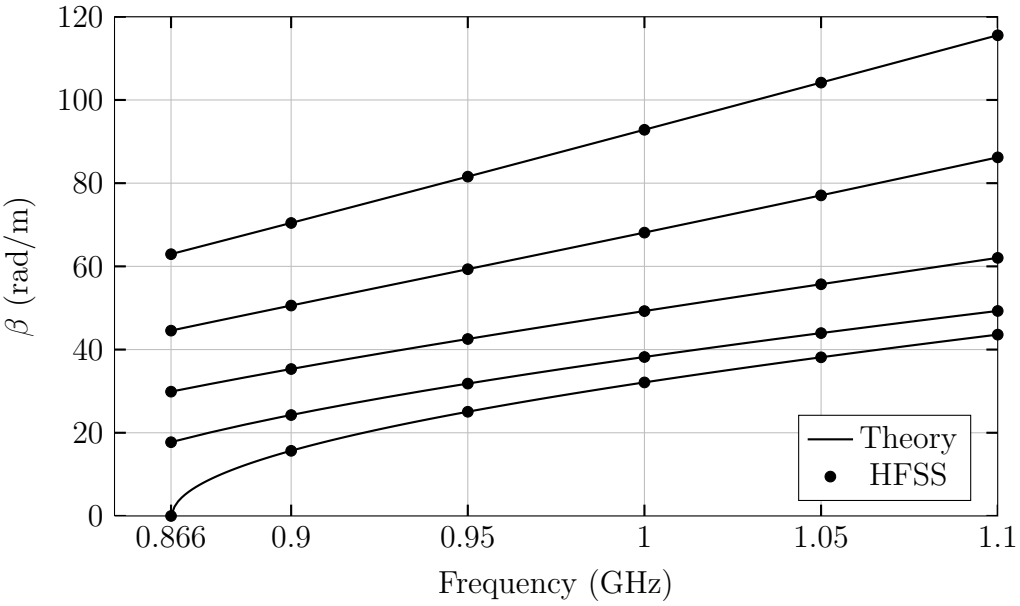

Figure 4.1: Frequency dependent phase constant determined using theory and HFSS for air (bottom) and a liquid permittivity of 20, 40, 60 and 80 (top). The probe parameters are $\epsilon_{\mathrm{r,Load}} = 9.74$, $a_n = 0.824$ and $b = 6.90$cm.

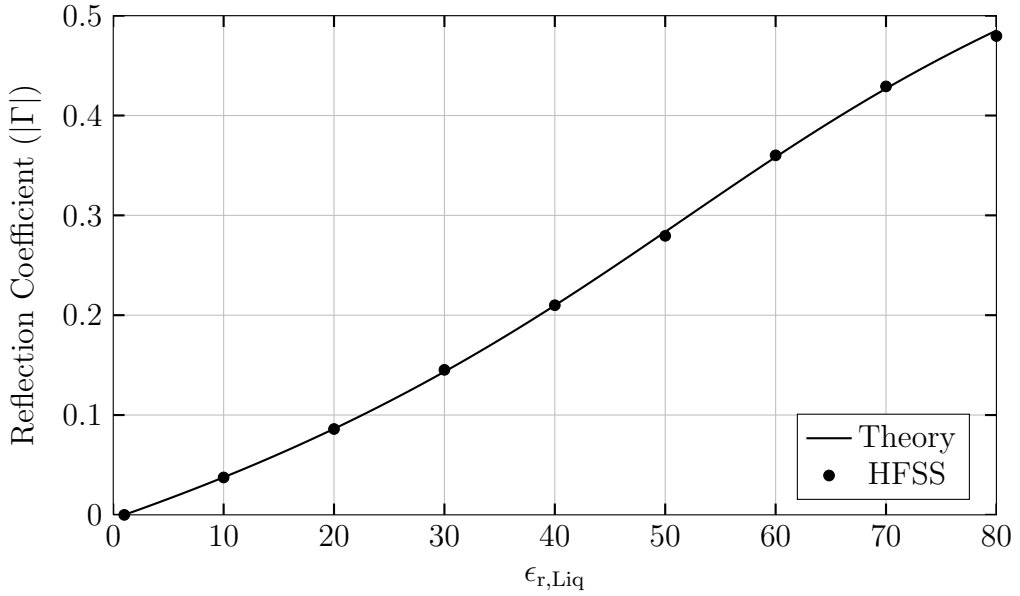

Figure 4.2: Magnitude of the reflection coefficient determined using theory and HFSS over the range of expected liquid permittivity values. The probe parameters are $\epsilon_{\mathrm{r,Load}} = 9.74$, $a_n = 0.824$ and $b = 6.90$cm.

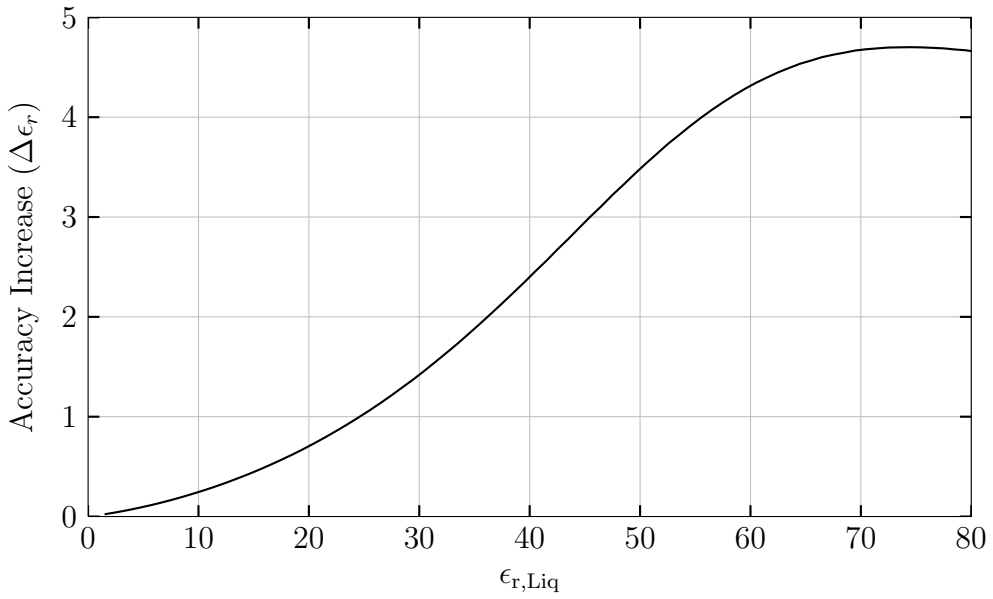

Figure 4.3: Permittivity accuracy increase over the range of expected liquid permittivity values. The probe has been optimized at $\epsilon_{r,\mathrm{Peak}} = 60$ for a liquid with a maximum relative permittivity of $\epsilon_{r,\mathrm{Max}} = 80$. The probe parameters are $\epsilon_{\mathrm{r,Load}} = 9.74$, $a_n = 0.824$ and $b = 6.90$cm. Accuracy increase is reported relative to a TEM probe.

Table 4.1: Summary of probe construction and performance parameters ($\epsilon_{r,\mathrm{Max}} = 80$, $\epsilon_{r,\mathrm{Peak}} = 60$, $A_{Tp} = 10^{-4}$, $L = 3$m, $f_{\mathrm{car}} = 1$GHz).

$h_{\min}$ (m)	$\epsilon_{\mathrm{r,Load}}$	a_n	b (cm)	$f_{\mathrm{car,n}}$	$f_{c,01}$ (GHz)	$f_{c,02}$ (GHz)	$\frac{v_{\mathrm{g,Liq}}}{c}$	$\beta''_{0,n}$ ($\times 10^{-18}$)	$\frac{\lvert\Gamma_{\mathrm{TE}}\rvert}{\lvert\Gamma_{\mathrm{TEM}}\rvert}$	Δh	$\Delta\epsilon_r$
1.0	9.74	0.824	6.90	0.58	0.866	1.100	0.175	-139	0.46	6.1	4.3
1.2	5.61	0.872	8.70	0.53	0.895	1.097	0.207	-125	0.51	5.2	5.4
1.4	3.63	0.899	10.57	0.50	0.911	1.088	0.237	-113	0.55	4.6	6.5
1.6	2.67	0.914	12.18	0.50	0.920	1.080	0.265	-99	0.57	4.2	7.4
1.8	2.14	0.923	13.49	0.50	0.929	1.077	0.287	-91	0.60	3.9	8.2
2.0	1.77	0.930	14.72	0.50	0.933	1.072	0.307	-84	0.62	3.7	8.9
2.2	1.51	0.936	15.95	0.50	0.934	1.066	0.326	-78	0.62	3.4	9.5
2.4	1.32	0.940	16.97	0.50	0.937	1.063	0.341	-74	0.63	3.3	10.0
2.6	1.17	0.944	18.03	0.50	0.939	1.061	0.358	-69	0.63	3.2	10.6
2.8	1.05	0.947	18.98	0.50	0.941	1.058	0.372	-66	0.64	3.1	11.1
2.91	1.00	0.948	19.39	0.50	0.943	1.057	0.378	-66	0.65	3.0	11.3

Table 4.2: Summary of probe construction and performance parameters ($\epsilon_{r,\mathrm{Max}} = 60$, $\epsilon_{r,\mathrm{Peak}} = 45$, $A_{Tp} = 10^{-4}$, $L = 3$m, $f_{\mathrm{car}} = 1$GHz).

$h_{\min}$ (m)	$\epsilon_{\mathrm{r,Load}}$	a_n	b (cm)	$f_{\mathrm{car,n}}$	$f_{c,01}$ (GHz)	$f_{c,02}$ (GHz)	$\frac{v_{\mathrm{g,Liq}}}{c}$	$\beta''_{0,n}$ ($\times 10^{-18}$)	$\frac{\lvert\Gamma_{\mathrm{TE}}\rvert}{\lvert\Gamma_{\mathrm{TEM}}\rvert}$	Δh	$\Delta\epsilon_r$
1.0	9.20	0.797	7.22	0.58	0.860	1.108	0.187	-116	0.47	5.8	3.5
1.2	5.17	0.856	9.14	0.53	0.890	1.105	0.222	-103	0.52	4.9	4.5
1.4	3.36	0.886	11.06	0.50	0.906	1.095	0.254	-94	0.56	4.3	5.3
1.6	2.46	0.904	12.78	0.50	0.914	1.086	0.284	-81	0.58	3.9	6.1
1.8	1.95	0.915	14.21	0.50	0.924	1.083	0.309	-74	0.60	3.6	6.8
2.0	1.62	0.923	15.53	0.50	0.927	1.077	0.330	-68	0.62	3.4	7.3
2.2	1.38	0.929	16.73	0.50	0.931	1.073	0.350	-63	0.63	3.2	7.8
2.4	1.20	0.934	17.88	0.50	0.932	1.068	0.368	-60	0.63	3.0	8.3
2.6	1.07	0.938	18.94	0.50	0.935	1.065	0.384	-57	0.64	2.9	8.7
2.72	1.00	0.940	19.53	0.50	0.936	1.064	0.393	-55	0.65	2.9	9.0

Table 4.3: Summary of probe construction and performance parameters ($\epsilon_{r,\mathrm{Max}} = 40$, $\epsilon_{r,\mathrm{Peak}} = 30$, $A_{Tp} = 10^{-4}$, $L = 3\mathrm{m}$, $f_{\mathrm{car}} = 1\mathrm{GHz}$).

$h_{\min}$ (m)	$\epsilon_{\mathrm{r,Load}}$	a_n	b (cm)	$f_{\mathrm{car,n}}$	$f_{c,01}$ (GHz)	$f_{c,02}$ (GHz)	$\frac{v_{\mathrm{g,Liq}}}{c}$	$\beta''_{0,n}$ ($\times 10^{-18}$)	$\frac{\lvert\Gamma_{\mathrm{TE}}\rvert}{\lvert\Gamma_{\mathrm{TEM}}\rvert}$	Δh	$\Delta\epsilon_r$
1.0	8.98	0.740	7.61	0.58	0.848	1.114	0.203	-93	0.48	5.4	2.6
1.2	4.72	0.826	9.80	0.52	0.874	1.108	0.243	-81	0.54	4.5	3.4
1.4	3.00	0.866	11.91	0.50	0.892	1.099	0.280	-71	0.58	3.9	4.1
1.6	2.19	0.888	13.74	0.50	0.903	1.092	0.313	-61	0.60	3.5	4.7
1.8	1.73	0.901	15.26	0.50	0.912	1.087	0.341	-55	0.62	3.2	5.2
2.0	1.44	0.910	16.62	0.50	0.918	1.083	0.364	-51	0.64	3.0	5.6
2.2	1.22	0.918	17.97	0.50	0.921	1.079	0.387	-47	0.64	2.9	6.0
2.4	1.07	0.923	19.08	0.50	0.927	1.076	0.405	-45	0.67	2.7	6.4
2.50	1.00	0.926	19.73	0.50	0.927	1.073	0.415	-43	0.66	2.7	6.5

The dielectric loading directly affects most probe parameters such as the group velocity in the liquid, dispersion, probe radius and the probe performance. It is shown that the minimum height is strongly correlated with the maximum group velocity in the liquid. For loadings with relative permittivity greater than 10 the benefit due to the reduction in group velocity in the liquid diminishes while dispersion continues to increase. As a result, it is not possible to achieve continuously lower minimum heights by increasing the dielectric loading. In the three above cases, this occurs for minimum heights below 1m. As expected, the probe radius is reduced with increasing dielectric loading by reducing the effective wavelength within the air filled region of the probe. Increasing dielectric loading results in an increase in height measurement accuracy as there is a direct correlation between the signal velocity in air and height measurements. Increasing the dielectric loading results in a decrease in the magnitude of the reflection coefficient, hence the permittivity accuracy is reduced. The increased dielectric loading effectively decreases the change in the impedance between the air and liquid filled regions. Smaller impedance change results in lower reflection coefficient magnitude and consequently permittivity measurement accuracy.

The amount of pulse spreading due to dispersion is evident in changes to the normalized carrier frequency and bandwidth requirement. Ideally, the normalized carrier frequency is 0.5 as this results in a carrier frequency halfway between the cutoff frequency of the fundamental mode in air and the cutoff frequency of the first higher order mode at the highest liquid permittivity considered. With this setting, all available bandwidth is used thereby allowing for the smallest duration of the time domain signal possible. However, dis-

persion increases as normalized carrier frequency decreases towards the cutoff frequency. Eventually, the benefit of optimally using the available bandwidth is negated by the increase in pulse spreading. When dispersion is high, still a lower minimum height can be achieved by increasing the normalized carrier frequency, at the expense of usable bandwidth. This is evident from the selection of the normalized carrier frequency equal to 0.58 at a minimum height of 1m in all three cases.

Fluids having a relative permittivity less than 30 have not been considered. At low values of relative permittivity the TEM reflection coefficient changes rapidly, thereby greatly reducing the opportunity for improvement using TE probes. Refer to Figure 2.2 for the TEM reflection coefficient.

4.2 Validating the Lossless Approximation on Lossy Liquids

In this section the validity of the lossless approximations will be investigated by applying it to water based solutions. In particular, ethanol-water and acetic acid solutions of varying concentrations have been investigated. Polar liquids, such as water and ethanol-water solutions can be modeled by the Debye relation [70],

$$\epsilon'(\omega) = \epsilon'_{\infty} + \frac{\epsilon'_s - \epsilon'_{\infty}}{1 + \omega^2 \tau_{Re}^2} \tag{4.1}$$

$$\epsilon''(\omega) = \frac{\omega \tau_{Im}(\epsilon'_s - \epsilon'_{\infty})}{1 + \omega^2 \tau_{Im}^2} \tag{4.2}$$

Where ϵ'_s is the real static permittivity at low frequency, ϵ'_{∞} is the real permittivity at very high frequency, τ_{Re} is the relaxation time corresponding to the real component of the permittivity, and τ_{Im} is the relaxation time corresponding to the imaginary component of the permittivity. For solutions that contain free ions, as is the case for acetic acid solutions, Equation 4.2 can be modified to include the conductivity (σ) [70],

$$\epsilon''(\omega) = \frac{\omega \tau_{Im}(\epsilon'_s - \epsilon'_{\infty})}{1 + \omega^2 \tau_{Im}^2} + \frac{\sigma}{\omega \epsilon_0} \tag{4.3}$$

Measurement of three parameters (liquid height, real and complex permittivity) cannot be done directly while using only the amplitude and delay of the first reflected signal. However, the real and imaginary components of the permittivity are directly related to the concentration of the solution. Thus, the liquid height and its concentration, based on the measurement of the real permittivity, can be determined. Such measurements are difficult using traditional TEM methods as the amplitude of the reflection coefficient may not vary significantly over the expected concentration of the solutions. Additionally, when the magnitude of the reflection coefficient is close to one, very little energy is able to penetrate into the liquid. As a result, complex permittivity measurements of such applications are difficult [71].

From the above equations, the dielectric properties are frequency dependent and therefore the reflection coefficient and concentration accuracy are

also frequency dependent. To investigate the impact of the frequency dependent liquid properties on measurements, probes have been compared at 1GHz and 5GHz carrier frequencies.

It is known that below the relaxation frequency of the liquid, dielectric losses will increase with increasing frequency, as determined by Equation 4.2 or 4.3. A carrier frequency of 1GHz is chosen as it represents the lowest frequency, and therefore lowest losses, that can be constructed with physically reasonable dimensions. The 5GHz carrier probe is used to investigate the performance where losses are considered high. The lossy data points have been determined with the simulation software, Ansoft HFSS, with the exception of the TEM case, which can be calculated using Equation 2.11.

4.2.1 Ethanol-Water Solutions

This section investigates the feasibility of measuring liquid height and the concentration of an ethanol-water solution using the results of the lossless method established previously. The required Debye parameters and subsequent real and imaginary components of permittivity have been calculated using experimentally derived equations in [39] and summarized in Table 4.4. The probe parameters have been optimized for a real permittivity midway between the expected concentration range of 0% to 40%.

Table 4.4: Dielectric properties of ethanol-water solutions at 1GHz and 5GHz at room temperature [39].

Ethanol	1GHz			5GHz		
Concentration	ϵ_r'	ϵ_r''	$\tan\delta$	ϵ_r'	ϵ_r''	$\tan\delta$
0%	79.19	3.74	0.047	74.46	17.54	0.236
5%	76.55	4.45	0.058	69.96	20.21	0.289
10%	73.89	5.10	0.069	65.36	22.36	0.342
20%	68.55	6.24	0.091	56.17	25.16	0.448
40%	57.80	7.88	0.136	39.42	25.97	0.659

4.2.1.1 Ethanol Concentration: Low Frequency Measurement (1GHz)

Two probe designs have been chosen for this investigation to establish the range of expected probe performance. These two designs represent the best

and worst case scenario for error introduced due to multiple reflections. Determining the optimum probe design requires determining the mode transfer coefficients and liquid attenuation which is beyond the scope of this thesis. The results for these probes are summarized in Table 4.5. The reflection coefficient over the range of real liquid permittivities is shown in Figure 4.4 with the increase in accuracy over the same range given in Figure 4.5. The lossy data points are summarized in Table 4.6.

Table 4.5: Summary of probe construction and performance parameters at 1GHz ($\epsilon_{r,\mathrm{Max}} = 79.20$, $\epsilon_{r,\mathrm{Peak}} = 68.50$, $A_{Tp} = 10^{-4}$, $L = 3\mathrm{m}$).

$h_{\min}$ (m)	$\epsilon_{\mathrm{r,Load}}$	a_n	b (cm)	$f_{\mathrm{car,n}}$	$f_{c,01}$ (GHz)	$f_{c,02}$ (GHz)	$\frac{v_{\mathrm{g,Liq}}}{c}$	$\beta''_{0,n}$ ($\times 10^{-18}$)	$\frac{\lvert\Gamma_{\mathrm{TE}}\rvert}{\lvert\Gamma_{\mathrm{TEM}}\rvert}$	Δh	$\Delta\epsilon_r$
-	1.00	0.953	20.00	0.61	0.914	1.054	0.43	-33.7	0.54	2.5	13.5
1	8.77	0.848	7.27	0.58	0.861	1.101	0.18	-119	0.46	5.8	5.1

The first design assumes the liquid is sufficiently lossy such that multiple reflections can be neglected, allowing for the lowest permittivity loading possible of $\epsilon_{\mathrm{r,Load}} = 1$. Alternatively, a matched termination could be used to reduce the amplitude of the reflections from the bottom of the probe. This results in an anticipated concentration accuracy increase of 13.5 times, and 2.5 times for height measurement over TEM measurement methods at the same frequency. With losses taken into account for both TE and TEM cases, the accuracy of concentration measurements is 11.0 times that of a TEM probe.

The second design assumes the worst case where no attenuation occurs and the permittivity loading must be chosen sufficiently high to ensure that multiple reflections are negligible, as would be the case for a lossless liquid. A total probe length of 3m with a minimum height of 1m has been used. This results in a loading permittivity of $\epsilon_{\mathrm{r,Load}} = 8.77$. This probe has an anticipated concentration accuracy increase of 5.1 times, and 5.8 times for height measurement over TEM measurement methods at the same frequency. With losses taken into account for both TE and TEM cases, the concentration accuracy is slightly decreased to 4.7 times that of a TEM probe.

By analyzing the results shown in Figure 4.4 the validity of the lossless approximation can be established. The introduction of losses results in a reduction of the magnitude of the reflection coefficient, however, the trend in

Table 4.6: Reflection properties of ethanol-water solutions at 1GHz and room temperature. (a) $\epsilon_{r,\text{Load}} = 1$ and (b) $\epsilon_{r,\text{Load}} = 8.77$.

Ethanol Concentration	$\lvert\Gamma_{\text{TEM}}\rvert$	$\lvert\Gamma_{\text{TE}}\rvert^{(a)}$	$\lvert\Gamma_{\text{TE}}\rvert^{(b)}$
0%	0.798	0.534	0.399
5%	0.795	0.489	0.378
10%	0.792	0.442	0.353
20%	0.785	0.356	0.323
40%	0.769	0.225	0.254

both probe designs agrees with the predicted results. The impact on the reduction in reflection coefficient magnitude due to the introduction of losses can be seen in Figure 4.4. The reduction of the magnitude of the reflection coefficient is dependent on many factors, including, the mode transfer coefficients and loss tangent. Without knowledge of the mode transfer coefficients, it can be inferred that the rate at which the losses increase, with increasing ethanol concentration, directly correlates with the reduction in the reflection coefficient. In other words, at low ethanol concentrations the losses are relatively low and result in a small deviation from the lossless prediction. The increase in concentration results in a rapid increase in the losses and consequently, the deviation from the lossless prediction. This results in a net increase in permittivity accuracy at low ethanol concentrations and a decrease in accuracy for mid to high concentrations. Furthermore, the TEM reflection coefficient increases as the losses are increased, therby effectively decreasing the sensitivity of the TEM probe. The dashed line, shown in Figure 4.5, illustrates the increase in accuracy compared to the lossless TEM reflection coefficient. It is shown that the introduction of losses to the TEM case results in an increase in permittivity measurement accuracy of the waveguide probe but does not affect the shape of the curve.

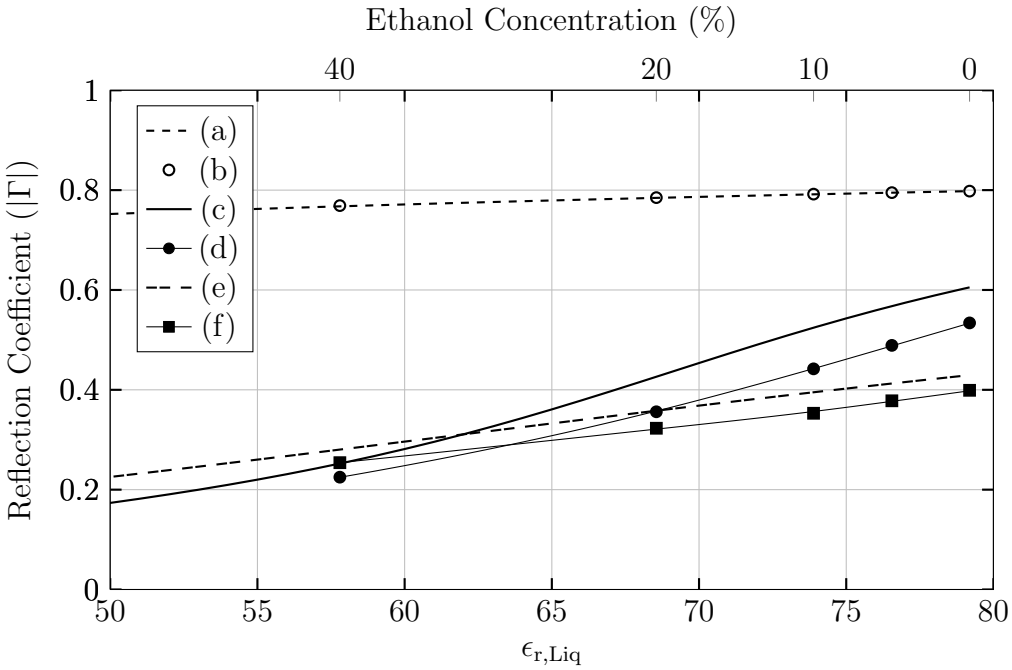

Figure 4.4: Reflection coefficient for lossless and lossy ethanol-water mixtures at 1GHz for (a) lossless TEM, (b) lossy TEM, (c) lossless $\epsilon_{r,\mathrm{Load}}$=1, (d) lossy $\epsilon_{r,\mathrm{Load}}$=1, (e) lossless $\epsilon_{r,\mathrm{Load}}$=8.77 and (f) lossy $\epsilon_{r,\mathrm{Load}}$=8.77.

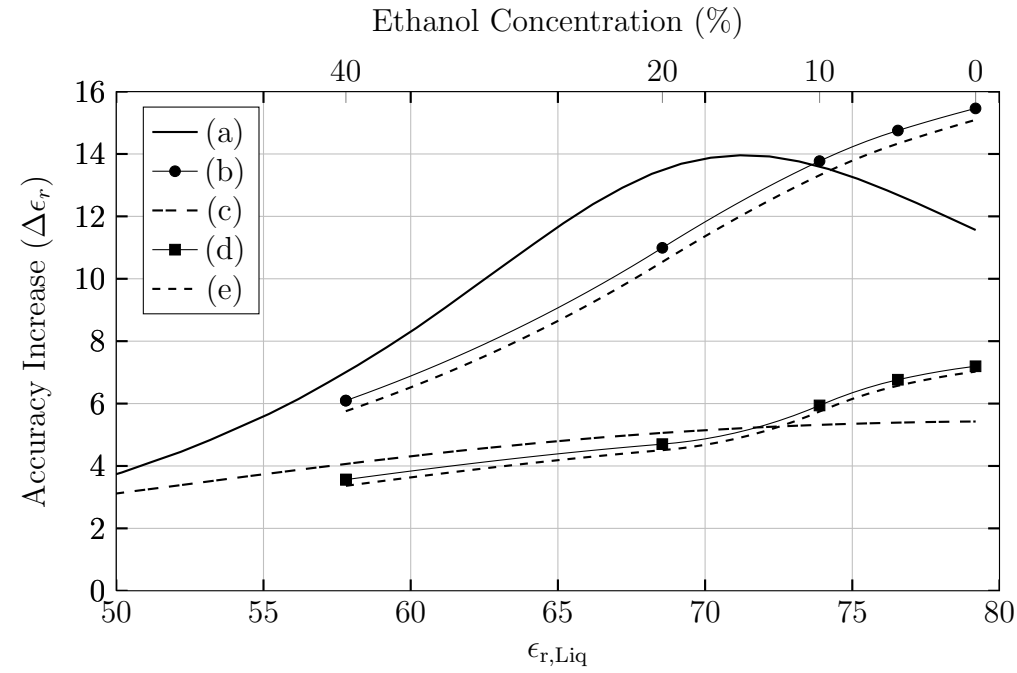

Figure 4.5: Permittivity accuracy increase at 1GHz for (a) lossless $\epsilon_{r,\mathrm{Load}}$=1, (b) lossy $\epsilon_{r,\mathrm{Load}}$=1, (c) lossless $\epsilon_{r,\mathrm{Load}}$=8.77, (d) lossy $\epsilon_{r,\mathrm{Load}}$=8.77 and (e) compared with lossless TEM.

4.2.1.2 Ethanol Concentration: High Frequency Measurement (5GHz)

An ethanol-water solution has been studied at 5GHz to determine the validity of the proposed method where losses are considered high. The resulting probe parameters as determined by the proposed optimization routine are given in Table 4.7. A probe with total length of 3m and minimum height of 1m would result in a carrier frequency of 4.88GHz at a permittivity loading of 1. Since the permittivity cannot be reduced any further, the dimensions of the probe can be reduced slightly to obtain a frequency of 5GHz, resulting in a minimum height of at most 98.8cm. Note that the minimum height would be significantly reduced if attenuation was included.

The reflection coefficient over the range of real permittivities of the liquid are shown in Figure 4.6 with the accuracy increase over the same range given in Figure 4.7. The lossy data points are summarized in Table 4.8.

Table 4.7: Summary of probe construction and performance parameters at 1GHz ($\epsilon_{r,\mathrm{Max}} = 74.46$, $\epsilon_{r,\mathrm{Peak}} = 56.94$, $A_{Tp} = 10^{-4}$, $L = 3$m).

$h_{\min}$ (m)	$\epsilon_{\mathrm{r,Load}}$	a_n	b (cm)	$f_{\mathrm{car,n}}$	$f_{c,01}$ (GHz)	$f_{c,02}$ (GHz)	$\frac{v_{\mathrm{g,Liq}}}{c}$	$\beta''_{0,n}$ ($\times 10^{-18}$)	$\frac{\lvert\Gamma_{\mathrm{TE}}\rvert}{\lvert\Gamma_{\mathrm{TEM}}\rvert}$	Δh	$\Delta\epsilon_r$
0.988	1.00	0.947	3.94	0.61	4.637	5.233	0.41	-44.1	0.62	2.7	11.3

Table 4.8: Reflection properties of ethanol-water solutions at 5GHz and room temperature.

Ethanol Concentration	$\lvert\Gamma_{\mathrm{TEM}}\rvert$	$\lvert\Gamma_{\mathrm{TE}}\rvert$
0%	0.796	0.437
5%	0.792	0.380
10%	0.788	0.335
20%	0.779	0.263
40%	0.756	0.166

The TEM reflection coefficient of a lossy liquid is greater than that of the lossless case. This effect is shown in Figure 4.6. Increased ethanol content in the solution results in a decrease in the real component of the permittivity and an increase in the loss tangent. For an ethanol concentration of 0%, corresponding to pure water, the reflection coefficient is 0.796 and 0.792 where losses are accounted for and neglected, respectively. Similarly, at 40%

ethanol concentration the reflection coefficient is 0.756 and 0.725 where losses are accounted for and neglected, respectively. If the losses are neglected, the reflection coefficient would vary by 0.071 over the concentration range of 0% to 40%. The actual reflection coefficient for the lossy solution varies by 0.036 over the concentration range of 0% to 40%. This decrease in the variation of the reflection coefficient when losses are present results in a decrease in measurement accuracy for a TEM probe. Consequently, a portion of the increase in accuracy of the TE probe is a result of this decrease in permittivity accuracy for the TEM probe. As discussed previously, the reflection coefficient of the TE probe decreases for lossy solutions due to energy transferred into higher order modes within the liquid. The net result is that TE probes can be used to provide increased measurement accuracy for lossy liquids. This is demonstrated in Figure 4.7. The dashed line, (c), corresponds to the predicted increase in accuracy of the TE probe compared to the reflection coefficient calculated when TEM losses are neglected. It has been shown that accounting for the losses of the liquid when calculating the TEM reflection coefficient results in both a more realistic approximation and an increase in permittivity measurement accuracy.

At a carrier frequency of 5GHz the high losses result in a significant reduction in the amplitude of the reflection coefficient. In both the 1GHz and 5GHz results, the loss tangent nearly triples over the increase in concentration from 0% to 40%. This rapid increase in both cases results in a similar reshaping of the reflection coefficient profile and the resulting accuracy increase. For permittivity values greater than 65 the accuracy of the lossy case exceeds that of the lossless case, corresponding to an improvement of 9.6 times that of a TEM probe at the same frequency. At the peak design permittivity the accuracy is decreased from 11.3 to 6.5 times that of a TEM probe at the same frequency.

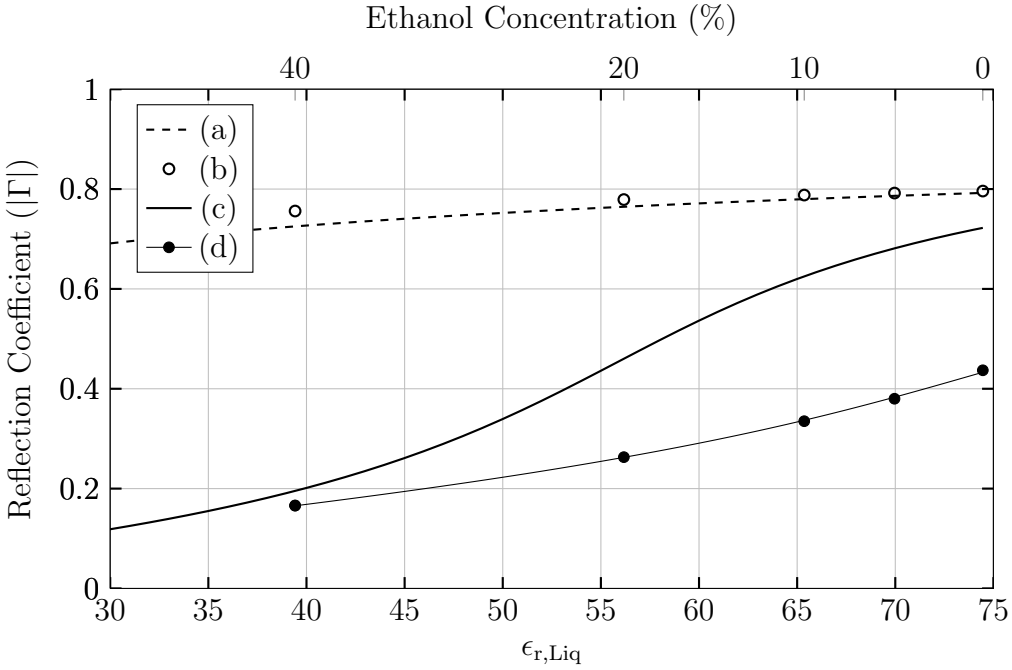

Figure 4.6: Reflection coefficient for lossless and lossy ethanol-water mixtures at 5GHz for (a) lossless TEM, (b) lossy TEM, (c) lossless $\epsilon_{r,\text{Load}}$=1 and (d) lossy $\epsilon_{r,\text{Load}}$=1.

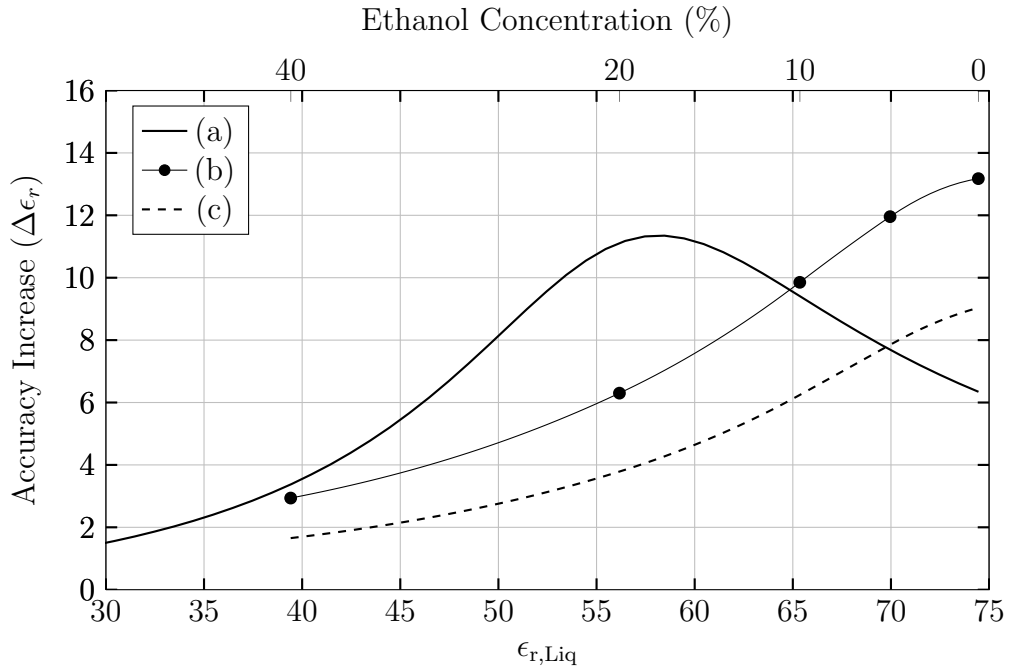

Figure 4.7: Permittivity accuracy increase at 5GHz for (a) lossless, (b) lossy and (c) compared with lossless TEM.

4.2.2 Acetic Acid Solutions

This section will investigate the feasibility of measuring liquid height and the concentration of an acetic acid solution using the results of the lossless method established previously. The required Debye parameters and subsequent real and imaginary components of permittivity have been calculated using experimentally derived equations in [40] and summarized in Table 4.9. The probe parameters have been optimized for a real permittivity midway between the expected concentration range of 0% to 10%.

Acetic acid solutions have been chosen to observe the impact of free ions on the frequency dependent permittivity and the resultant reflection coefficient. The impact of these free ions have been shown to have a significant correlation to the performance of the probe. Additionally, the magnitude of the reflection coefficient varies by 1% or less for TEM probes, which makes measurement difficult and allows for greater opportunity for improvement with TE probes.

Table 4.9: Dielectric properties of acetic acid solutions at 1GHz and 5GHz at room temperature [40].

Acetic Acid	1GHz			5GHz		
Concentration	ϵ_r'	ϵ_r''	$\tan\delta$	ϵ_r'	ϵ_r''	$\tan\delta$
0%	78.29	4.51	0.058	73.68	17.59	0.239
2%	77.25	5.54	0.072	72.16	17.78	0.246
4%	76.21	6.55	0.086	70.66	17.91	0.254
6%	75.16	7.56	0.101	69.19	17.99	0.260
8%	74.12	8.55	0.115	67.76	18.00	0.266
10%	73.08	9.52	0.130	66.36	17.95	0.271

4.2.2.1 Acetic Acid: Low Frequency Measurement (1GHz)

Again two probe designs have been proposed for the low loss approximation. The results are given in Table 4.10. The reflection coefficient over the range of real liquid permittivities is shown in Figure 4.8 with the accuracy increase over the same range given in Figure 4.9. The lossy data points are summarized in Table 4.11.

Where multiple reflections can be neglected a permittivity loading of 1 can be used, resulting in an anticipated accuracy increase of 15.0 and a height

Table 4.10: Summary of probe construction and performance parameters at 1GHz ($\epsilon_{r,\mathrm{Max}} = 78.29$, $\epsilon_{r,\mathrm{Peak}} = 75.69$, $A_{Tp} = 10^{-4}$, $L = 3$m).

$h_{\min}$ (m)	$\epsilon_{\mathrm{r,Load}}$	a_n	b (cm)	$f_{\mathrm{car,n}}$	$f_{c,01}$ (GHz)	$f_{c,02}$ (GHz)	$\frac{v_{\mathrm{g,Liq}}}{c}$	$\beta''_{0,n}$ ($\times 10^{-18}$)	$\frac{\lvert\Gamma_{\mathrm{TE}}\rvert}{\lvert\Gamma_{\mathrm{TEM}}\rvert}$	Δh	$\Delta\epsilon_r$
-	1.00	0.956	20.33	0.60	0.899	1.067	0.451	-25.3	0.51	2.3	15.0
1	7.86	0.866	7.64	0.57	0.862	1.112	0.192	-104	0.45	5.4	5.8

Table 4.11: Reflection properties of acetic acid solutions at 1GHz and room temperature. (a) $\epsilon_{r,\mathrm{Load}} = 1$ and (b) $\epsilon_{r,\mathrm{Load}} = 7.86$.

Acetic Acid Concentration	$\lvert\Gamma_{\mathrm{TEM}}\rvert$	$\lvert\Gamma_{\mathrm{TE}}\rvert^{(a)}$	$\lvert\Gamma_{\mathrm{TE}}\rvert^{(b)}$
0%	0.797	0.375	0.349
2%	0.796	0.348	0.338
4%	0.795	0.323	0.327
6%	0.794	0.301	0.315
8%	0.793	0.283	0.306
10%	0.792	0.265	0.296

accuracy of 2.3 times over that of a TEM probe at the same frequency. With multiple reflections accounted for, a permittivity loading of 7.86 is required. This results in a permittivity accuracy increase of 5.8 and a height accuracy increase of 5.4 times that of a TEM probe at the same frequency.

When losses are taken into account, the permittivity accuracy is increased to 20.2 and 10.0 respectively for the two probes. This increase in accuracy can be attributed to the impact of free ions at low frequencies. The presence of free ions results in a rapid increase in the loss tangent at low frequencies as the concentration is increased from 0% to 10%. This results in a similar effect to the ethanol-water probes, however, since the loss tangent quickly increases over a small range of liquid permittivity values, the result is a net increase in accuracy over the range of interest. Additionally, the relatively high loss tangent has a noticeable affect on the TEM reflection coefficient and consequently the accuracy improvement. This effect is shown by the dashed line, (e), in Figure 4.9.

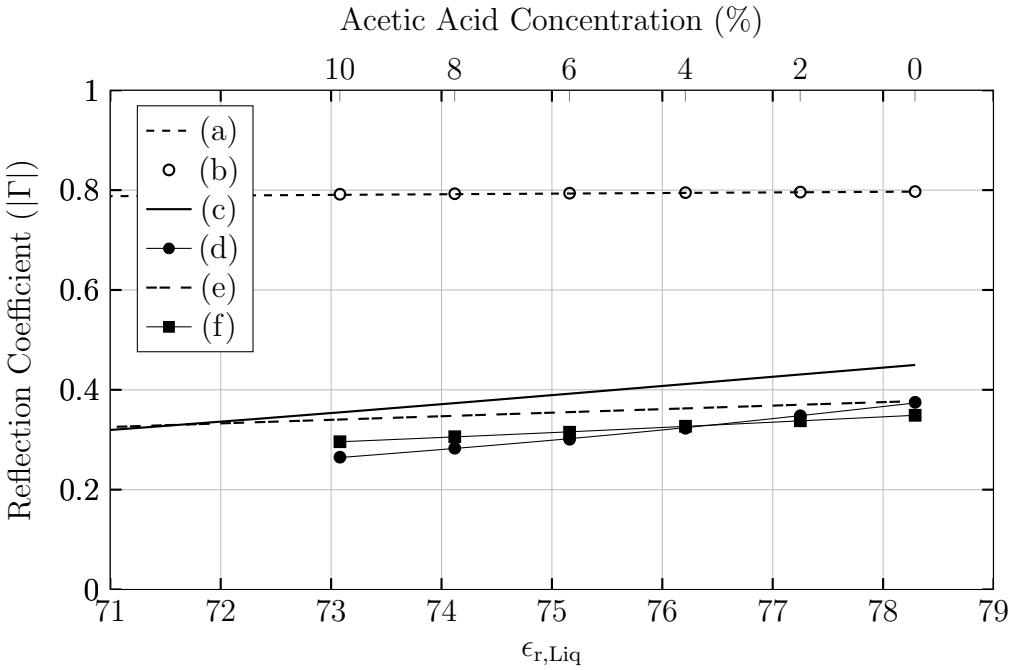

Figure 4.8: Reflection coefficient for lossless and lossy acetic acid mixtures at 1GHz, (a) lossless TEM, (b) lossy TEM, (c) lossless $\epsilon_{r,\mathrm{Load}}$=1, (d) lossy $\epsilon_{r,\mathrm{Load}}$=1, (e) lossless $\epsilon_{r,\mathrm{Load}}$=7.86 and (f) lossy $\epsilon_{r,\mathrm{Load}}$=7.86.

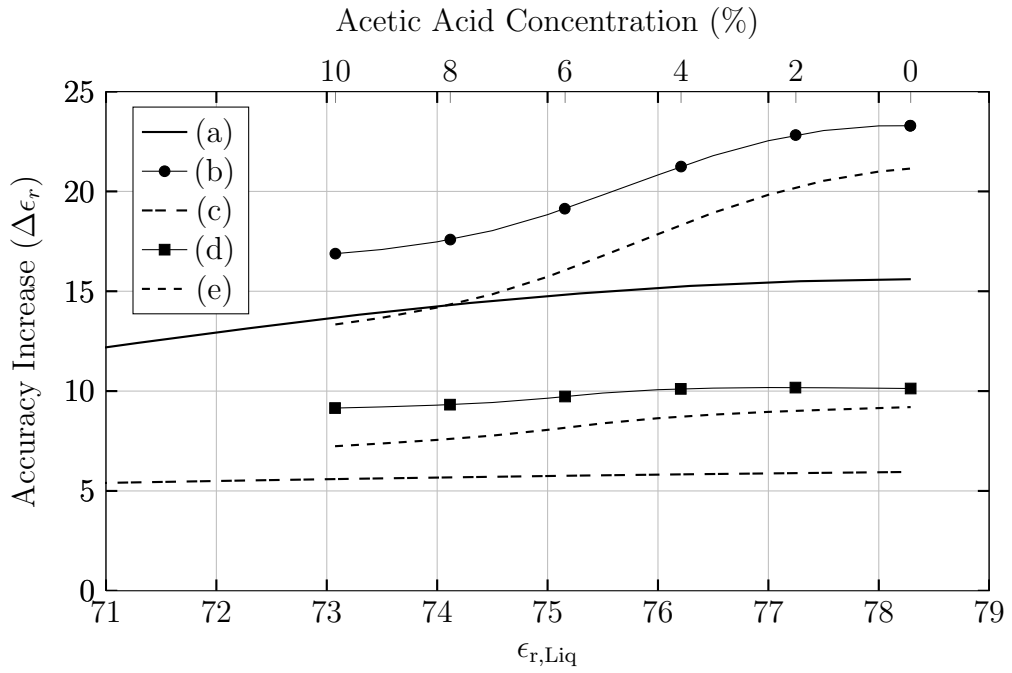

Figure 4.9: Permittivity accuracy increase at 1GHz for (a) lossless $\epsilon_{r,\mathrm{Load}}$=1, (b) lossy $\epsilon_{r,\mathrm{Load}}$=1, (c) lossless $\epsilon_{r,\mathrm{Load}}$=7.86, (d) lossy $\epsilon_{r,\mathrm{Load}}$=7.86 and (e) compared with lossless TEM.

4.2.2.2 Acetic Acid: High Frequency Measurement (5GHz)

In this section, the frequency is increased to 5GHz where the impact of free ions are negligible, but polar losses remain high. A permittivity loading of 1 results in a carrier frequency of 3.69GHz for a minimum height of 1m on a probe with a total length of 3m. To increase the operating frequency to 5GHz the radius has been reduced from 5.48cm to 4.07cm and the normalized carrier frequency increased from 0.59 to 0.63. This results in a decrease in minimum height from 1m to 86.1cm. Alternatively, the normalized carrier frequency could be increased from 0.59 to 0.73 to operate at 5GHz with a minimum height of 1m, which would also result in a slight increase in permittivity accuracy from 14.2 to 14.5. The former has been used as the reduction in minimum height is more significant than the increase in permittivity measurement accuracy.

Table 4.12: Summary of probe construction and performance parameters at 5GHz ($\epsilon_{r,\mathrm{Max}} = 73.68$, $\epsilon_{r,\mathrm{Peak}} = 70.02$, $A_{Tp} = 10^{-4}$, $L = 3$m).

$h_{\min}$ (m)	$\epsilon_{\mathrm{r,Load}}$	a_n	b (cm)	$f_{\mathrm{car,n}}$	$f_{c,01}$ (GHz)	$f_{c,02}$ (GHz)	$\frac{v_{\mathrm{g,Liq}}}{c}$	$\beta''_{0,n}$ ($\times 10^{-18}$)	$\frac{\lvert\Gamma_{\mathrm{TE}}\rvert}{\lvert\Gamma_{\mathrm{TEM}}\rvert}$	Δh	$\Delta\epsilon_r$
0.861	1.00	0.954	4.07	0.63	4.488	5.304	0.455	-24.4	0.53	2.3	14.2

Table 4.13: Reflection properties of acetic acid solutions at 5GHz and room temperature.

Acetic Acid Concentration	$\lvert\Gamma_{\mathrm{TEM}}\rvert$	$\lvert\Gamma_{\mathrm{TE}}\rvert$
0%	0.795	0.242
2%	0.794	0.233
4%	0.792	0.224
6%	0.790	0.215
8%	0.788	0.207
10%	0.787	0.199

From Table 4.9 it is evident that an increase in concentration does not have a significant impact on the losses present. Increasing the concentration from 0% to 10% results in an increase in the loss tangent from 0.239 to 0.279. Consequently, the accuracy is reduced from 14.2 to 4.9 times that of a TEM probe at the same frequency. It has been concluded that when the losses are high and the losses do not vary significantly over the range of interest the results do not agree with those predicted by the lossless assumption.

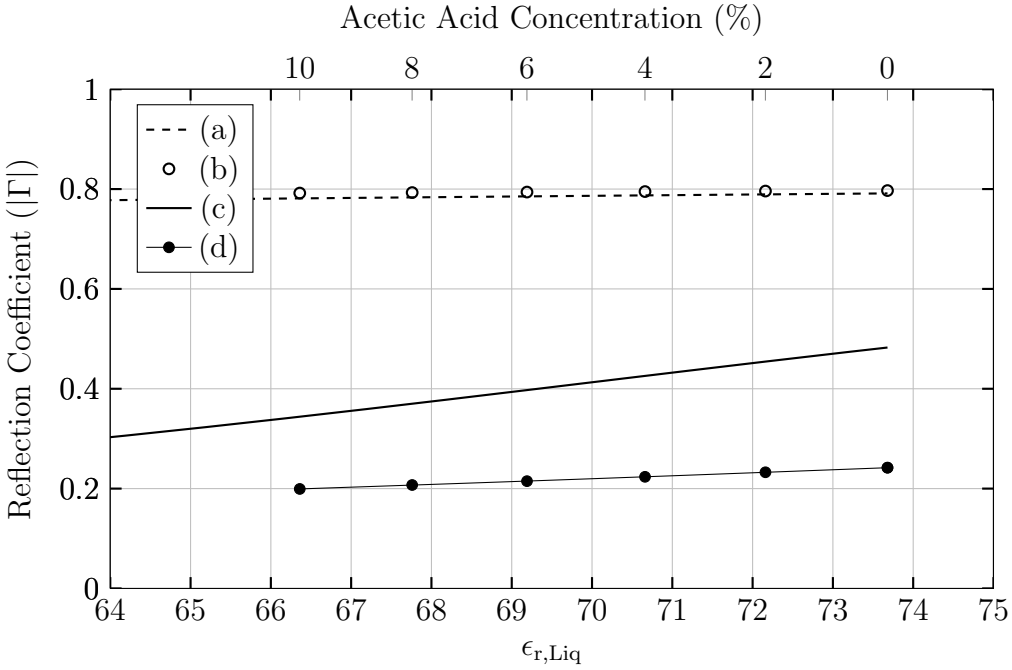

Figure 4.10: Reflection coefficient for lossless and lossy acetic acid mixtures at 5GHz, (a) lossless TEM, (b) lossy TEM, (c) lossless $\epsilon_{r,\mathrm{Load}}$=1 and (d) lossy $\epsilon_{r,\mathrm{Load}}$=1.

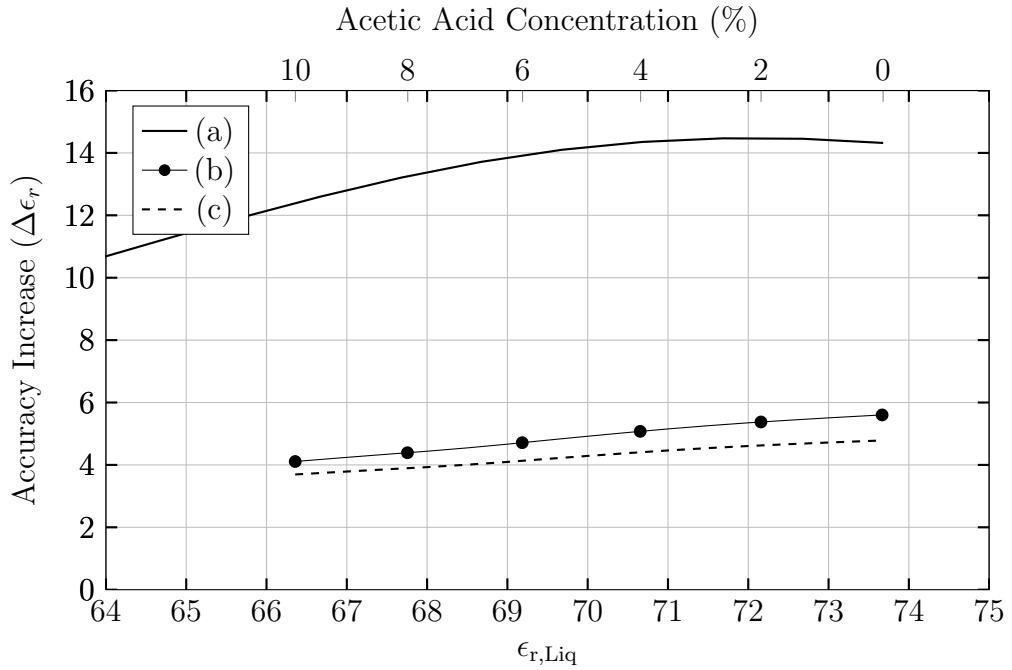

Figure 4.11: Permittivity accuracy increase at 5GHz for (a) lossless, (b) lossy and (c) compared with lossless TEM.

Chapter 5

Summary and Future Recommendations

A probe optimization procedure has been developed to determine the parameters of a dielectric loaded circular waveguide probe that utilizes the TE_{01} mode for TDR applications. It has been found that fluids having a relative permittivity greater than 30 are able to be more accurately characterized using the proposed TE probes. For fluids with a relative permittivity below 30, the TEM reflection coefficient changes rapidly, therefore, significant accuracy improvements are not feasible. For all liquid applications it has been found that the proposed probes provide increased height measurement accuracy proportional to the dielectric constant of the loading material. Although the optimization procedure uses a lossless assumption, the resulting probe designs have been shown to provide improved accuracy over TEM probes in lossy applications.

Ethanol-water and acetic acid solutions were chosen to investigate the validity of the lossless optimization procedure for lossy applications. It was found that the magnitude of the losses and the rate at which the losses increase determine the performance of the probe. The presence of free ions results in a rapid change in losses at low frequencies. This results in a significant increase in permittivity accuracy at low frequencies and a significant drop in permittivity accuracy at high frequencies. At 1GHz the measurement of the concentration of an ethanol-water solution ranges from 4.7 to 11.0 times greater than that of a TEM probe, depending on the dielectric loading used and the minimum height required. Similarly, at 1GHz the measurement of the concentration of an acetic acid solution ranges from 10.0 to 20.2 times greater than that of a

TEM probe, depending on the dielectric loading used and the minimum height required. In both cases losses have been taken into account using simulation results from Ansoft HFSS. The losses of the liquid do not have an impact on the height measurement accuracy. The permittivity accuracy exceeded that of the TEM probe in all cases considered.

The optimization procedure accounts for the dispersive nature of waveguide probes, multiple reflections within the fluid and ensures monomode operation while meeting the minimum height of the fluid for a particular application. A probe length of 3m with a minimum height of 1m has been assumed, except where otherwise stated. This probe length is typical for an industrial application. A minimum height of 1m is significantly larger than that of a TEM probe, however, this conservative value could be reduced by accounting for the attenuation of the fluid, utilizing a matched termination or by implementing dispersion compensation methods. Dispersion could be reduced by utilizing a signal that has a better time-bandwidth product, such as a secant-squared pulse. A signal that is chirped proportional to the anticipated height of the liquid could result in pulse compression rather than pulse spreading, thereby reducing the minimum height. The optimization procedure could be further improved by incorporating the expected losses of the liquid while calculating the reflection coefficient.

References

[1] Hugo Fellner-Feldegg. Measurement of dielectrics in the time domain. *The Journal of Physical Chemistry*, 73(3):616–623, 1969.

[2] G. C. Topp, J. L. Davis, and A. P. Annan. Electromagnetic determination of soil water content: measurements in coaxial transmission lines. *Water Resources Research*, 16(3):574–582, 1980.

[3] F. N. Dalton and M. Th. Van Genuchten. The time-domain reflectometry method for measuring soil water content and salinity. *Geoderma*, 38(1):237–250, 1986.

[4] D. A. Robinson, Scott B. Jones, J. M. Wraith, D. Or, and S. P. Friedman. A review of advances in dielectric and electrical conductivity measurement in soils using time domain reflectometry. *Vadose Zone Journal*, 2(4):444–475, 2003.

[5] K. Noborio. Measurement of soil water content and electrical conductivity by time domain reflectometry: a review. *Computers and electronics in agriculture*, 31(3):213–237, 2001.

[6] Scott B. Jones, Jon M. Wraith, and Dani Or. Time domain reflectometry measurement principles and applications. *Hydrological Processes*, 16(1):141–153, 2002.

[7] H. Fluhler, M. Nussberger, W. Bächtold, H. Benedickter, and H. Wunderli. Single-rod probes for time domain reflectometry: sensitivity and calibration. In *AGU Fall Meeting Abstracts*, volume 1, page 0408, 2004.

[8] David Moret-Fernández, F. Lera, J. L. Arrúe, and M. V. López. Measurement of soil bulk electrical conductivity using partially coated TDR probes. *Vadose Zone Journal*, 8(3):594–600, 2009.

[9] P. A. Ferré, D. L. Rudolph, and R. G. Kachanoski. Spatial averaging of water content by time domain reflectometry: Implications for twin rod probes with and without dielectric coatings. *Water Resources Research*, 32(2):271–279, 1996.

[10] John S. Selker, Lynette Graff, and Tammo Steenhuis. Noninvasive time domain reflectometry moisture measurement probe. *Soil Science Society of America Journal*, 57(4):934–936, 1993.

[11] Murray Lungal and Bing Cheng Si. Coiled time domain reflectometry matric potential sensor. *Soil Science Society of America Journal*, 72(5):1422–1424, 2008.

[12] Shin Yagihara, Mikio Oyama, Akio Inoue, Megumi Asano, Seiichi Sudo, and Naoki Shinyashiki. Dielectric relaxation measurement and analysis of restricted water structure in rice kernels. *Measurement Science and Technology*, 18(4):983, 2007.

[13] G. Murtaza Hashmi, Ruslan Papazyan, and Matti Lehtonen. Comparing wave propagation characteristics of MV XLPE cable and covered-conductor overhead line using time domain reflectometry technique. In *Electrical Engineering, 2007. ICEE'07. International Conference on*, pages 1–6. IEEE, 2007.

[14] Zsigmond M. Pal and Ronald H. Johnston. Simulation of pipeline holiday detection by time domain reflectometry. In *Petroleum and Chemical Industry Conference, 1989, Record of Conference Papers.. Industrial Applications Society, 36th Annual*, pages 103–108. IEEE, 1989.

[15] Renyuan Tong, Ming Li, and Qing Li. Design of elastic helical time domain reflectometry cable for distributed tensile deformation monitoring. In *Artificial Intelligence, Management Science and Electronic Commerce (AIMSEC), 2011 2nd International Conference on*, pages 3887–3890. IEEE, 2011.

[16] R. E. Patfterson and Neilson A. M. Mackay. A guided radar system for obstacle detection. *Instrumentation and Measurement, IEEE Transactions on*, 26(2):137–143, 1977.

[17] Alexander Scheuermann and Christof Huebner. On the feasibility of pressure profile measurements with time-domain reflectometry. *Instrumentation and Measurement, IEEE Transactions on*, 58(2):467–474, 2009.

[18] Te-Wen Pan, Ching-Wen Hsue, and Jhin-Fang Huang. Time-domain reflectometry using arbitrary incident waveforms. *Microwave Theory and Techniques, IEEE Transactions on*, 50(11):2558–2563, 2002.

[19] Andrew P. Gregory and Robert N. Clarke. A review of RF and microwave techniques for dielectric measurements on polar liquids. *Dielectrics and Electrical Insulation, IEEE Transactions on*, 13(4):727–743, 2006.

[20] D. K. Ghodgaonkar, V. V. Varadan, and V. K. Varadan. Free-space measurement of complex permittivity and complex permeability of magnetic materials at microwave frequencies. *Instrumentation and Measurement, IEEE Transactions on*, 39(2):387–394, 1990.

[21] S. Roberts and A. Von Hippel. A new method for measuring dielectric constant and loss in the range of centimeter waves. *Journal of Applied Physics*, 17(7):610–616, 1946.

[22] Leo P. Ligthart. A fast computational technique for accurate permittivity determination using transmission line methods. *Microwave Theory and Techniques, IEEE Transactions on*, 31(3):249–254, 1983.

[23] Ugur Cem Hasar. A fast and accurate amplitude-only transmission-reflection method for complex permittivity determination of lossy materials. *Microwave Theory and Techniques, IEEE Transactions on*, 56(9):2129–2135, 2008.

[24] Christopher Anderson. *Determining the complex permittivity of materials with the waveguide-cutoff method.* PhD thesis, 2006.

[25] Yoshio Kobayashi and Masayuki Katoh. Microwave measurement of dielectric properties of low-loss materials by the dielectric rod resonator method. *Microwave Theory and Techniques, IEEE Transactions on*, 33(7):586–592, 1985.

[26] Stanley S. Stuchly, M. A. K. Hamid, and Adolf Andres. Microwave surface level monitor. *Industrial Electronics and Control Instrumentation, IEEE Transactions on*, (3):85–92, 1971.

[27] Matthias Weib and Reinhard Knochel. A sub-millimeter accurate microwave multilevel gauging system for liquids in tanks. *Microwave Theory and Techniques, IEEE Transactions on*, 49(2):381–384, 2001.

[28] Matthias Weib and Reinhard Knochel. A highly accurate multi-target microwave ranging system for measuring liquid levels in tanks. In *Microwave Conference, 1997. 27th European*, volume 2, pages 1103–1112. IEEE, 1997.

[29] Seung Ho Doo, Won-Sang Ra, Tae Sung Yoon, and Jin Bae Park. Fast time-frequency domain reflectometry based on the AR coefficient estimation of a chirp signal. In *American Control Conference, 2009. ACC'09.*, pages 3423–3428. IEEE, 2009.

[30] Andrea Cataldo, Luca Catarinucci, Luciano Tarricone, Filippo Attivissimo, and Emanuele Piuzzi. A combined TD–FD method for enhanced reflectometry measurements in liquid quality monitoring. *Instrumentation and Measurement, IEEE Transactions on*, 58(10):3534–3543, 2009.

[31] C. Negrea and M. Rangu. Sequential sampling time domain reflectometer. In *15th International Symposium for Design and Technology of Electronics Packages, (SIITME) 2009*, pages 367–371. IEEE, 2009.

[32] Zhihong Ma and Seichi Okamura. Permittivity determination using amplitudes of transmission and reflection coefficients at microwave frequency. *Microwave Theory and Techniques, IEEE Transactions on*, 47(5):546–550, 1999.

[33] A. Cataldo, L. Tarricone, A. Trotta, F. Attivissimo, and C. Urso. Time domain reflectometry technique for monitoring of liquid characteristics. In *Instrumentation and Measurement Technology Conference, 2005. IMTC 2005. Proceedings of the IEEE*, volume 3, pages 1932–1936. IEEE, 2005.

[34] A. C. Nunes, X. Bohigas, and J. Tejada. Dielectric study of milk for frequencies between 1 and 20GHz. *Journal of food engineering*, 76(2):250–255, 2006.

[35] Wenchuan Guo, Xinhua Zhu, Hui Liu, Rong Yue, and Shaojin Wang. Effects of milk concentration and freshness on microwave dielectric properties. *Journal of Food Engineering*, 99(3):344–350, 2010.

[36] Masaki Kouzai, Atsuhiro Nishikata, Shunsuke Miyaoka, and Kaori Fukunaga. Fermentation process monitoring of Japanese sake by dielectric measurement. In *Dielectric Liquids, 2008. ICDL 2008. IEEE International Conference on*, pages 1–4. IEEE, 2008.

[37] Arvind V. Sarode and Ashok C. Kumbharkhane. Study of dielectric relaxation and thermodynamic behaviour in poly (propylene glycol) using time domain reflectometry. *Journal of Molecular Liquids*, 160(2):109–113, 2011.

[38] Y. S. Joshi, P. G. Hudge, A. C. Kumbharkhane, and S. C. Mehrotra. The dielectric relaxation study of 2 (2-alkoxyethoxy) ethanol–water mixtures using time domain reflectometry. *Journal of Molecular Liquids*, 163(2):70–76, 2011.

[39] Xavier Bohigas and Javier Tejada. Dielectric characterization of alcoholic beverages and solutions of ethanol in water under microwave radiation in the 1–20GHz range. *Food Research International*, 43(6):1607–1613, 2010.

[40] Xavier Bohigas and Javier Tejada. Dielectric properties of acetic acid and vinegar in the microwave frequencies range 1–20GHz. *Journal of Food Engineering*, 94(1):46–51, 2009.

[41] Christopher P. Nemarich. Time domain reflectometry liquid level sensors. *Instrumentation & Measurement Magazine, IEEE*, 4(4):40–44, 2001.

[42] Andrea Cataldo, Luciano Tarricone, Filippo Attivissimo, and Amerigo Trotta. A TDR method for real-time monitoring of liquids. *Instrumentation and Measurement, IEEE Transactions on*, 56(5):1616–1625, 2007.

[43] A. Cataldo, L. Tarricone, M. Vallone, F. Attivissimo, and A. Trotta. An assessment on the accuracy of time-domain reflectometry for measuring level and permittivity of liquids. In *Instrumentation and Measurement Technology Conference, 2006. IMTC 2006. Proceedings of the IEEE*, pages 2332–2337. IEEE, 2006.

[44] Andrea Cataldo, Luciano Tarricone, M. Vallone, Filippo Attivissimo, and Amerigo Trotta. Uncertainty estimation in simultaneous measurements of levels and permittivities of liquids using TDR technique. *Instrumentation and Measurement, IEEE Transactions on*, 57(3):454–466, 2008.

[45] W. Guo, S. S. Stuchly, and K. Caputa. Transmission media for microwave level gauging systems. *Journal of microwave power and electromagnetic energy*, 30(3):149–157, 1995. 388.

[46] B. Oswald, H. R. Benedickter, W Bächtold, and H. Flühler. A single-rod probe for time domain reflectometry measurements of the water content. *Vadose Zone Journal*, 3(4):1152–1159, 2004.

[47] Murray Lungal and Bing Cheng Si. Coiled time domain reflectometry matric potential sensor. *Soil Science Society of America Journal*, 72(5):1422–1424, 2008.

[48] David M. Pozar. *Microwave engineering*, volume 3. John Wiley&Son In, 2005.

[49] Annamaria Cereti, Elena Pettinelli, Alessandro Galli, and Francesco Bella. Shorted-end probes for accurate permittivity measurements with time-domain reflectometry. *Applied physics letters*, 83(5):1050–1052, 2003.

[50] U. C. Hasar, C. R. Westgate, and M. Ertugrul. Permittivity determination of liquid materials using waveguide measurements for industrial applications. *IET microwaves, antennas & propagation*, 4(1):141–152, 2010.

[51] Sergey N. Kharkovsky, M. Fatih Akay, Ugur Cem Hasar, and Cengiz Duran Atis. Measurement and monitoring of microwave reflection and transmission properties of cement-based specimens. *Instrumentation and Measurement, IEEE Transactions on*, 51(6):1210–1218, 2002.

[52] T. Lasri, D. Glay, L. Achrait, A. Mamouni, and Y. Leroy. Microwave methods and systems for nondestructive control. *Subsurface Sensing Technologies and Applications*, 1(1):141–160, 2000.

[53] Agilent Technologies Inc. High precision time domain reflectometry, application note 1304-7. Oct. 2007.

[54] David Jeffrey Griffiths and Reed College. *Introduction to electrodynamics*, volume 3. prentice Hall Upper Saddle River, NJ, 1999.

[55] Kawthar A Zaki, Chen Seng-Woon, and Chen Chunming. Modeling discontinuities in dielectric-loaded waveguides. *Microwave Theory and Techniques, IEEE Transactions on*, 36(12):1804–1810, 1988.

[56] Ll G. Chambers. Propagation in waveguides filled longitudinally with two or more dielectrics. *British Journal of Applied Physics*, 4(2):39, 1953.

[57] Abbas Sayed Omar and K. F. Schunemann. Complex and backward-wave modes in inhomogeneously and anisotropically filled waveguides. *Microwave Theory and Techniques, IEEE Transactions on*, 35(3):268–275, 1987.

[58] L. Pincherle. Electromagnetic waves in metal tubes filled longitudinally with two dielectrics. *Physical Review*, 66(5-6):118, 1944.

[59] Wansheng Su, Ioannis M. Besieris, and Sedki M. Riad. Velocity of an RF pulse signal propagating in a waveguide. *Microwave and Guided Wave Letters, IEEE*, 2(6):255–256, 1992.

[60] Radim Zajicek, Tomas Smejkal, Ladislav Oppl, and Jan Vrba. Waveguide probes for complex permittivity measurement. In *Microwave Techniques, 2008. COMITE 2008. 14th Conference on*, pages 1–4. IEEE, 2008.

[61] Steven L. Dvorak. Exact, closed-form expressions for transient fields in homogeneously filled waveguides. *Microwave Theory and Techniques, IEEE Transactions on*, 42(11):2164–2170, 1994.

[62] M. Ito. Dispersion of very short microwave pulses in waveguide. *Microwave Theory and Techniques, IEEE Transactions on*, 13(3):357–364, 1965.

[63] Sophocles J. Orfanidis. *Electromagnetic waves and antennas*. Rutgers University, 2002.

[64] P. Lazaridis, G. Debarge, and P. Gallion. Time-bandwidth product of chirped sech^2 pulses: application to phase-amplitude-coupling factor measurement. *Optics letters*, 20(10):1160–1162, 1995.

[65] Alvin Wexler. Solution of waveguide discontinuities by modal analysis. *Microwave Theory and Techniques, IEEE Transactions on*, 15(9):508–517, 1967.

[66] James Baker-Jarvis. *Transmission/reflection and short-circuit line permittivity measurements*. National Institute of Standards and Technology Colorado, 1990.

[67] E. Nagelberg and J. Shefer. *Mode conversion in circular waveguides*. Bell Telephone Laboratories, 1965.

[68] Mitsunobu Miyagi and Shigeo Nishida. Pulse spreading in a single-mode fiber due to third-order dispersion. *Applied optics*, 18(5):678–682, 1979.

[69] William M. Haynes, David R. Lide, and Thomas J. Bruno. *CRC handbook of chemistry and physics 2012-2013*. CRC press, 2012.

[70] Arthur R. Von Hippel. *Dielectric materials and applications. Papers by 22 contributors*. New York, 1954.

[71] Radim Zajíček, Ladislav Oppl, and Jan Vrba. Broadband measurement of complex permittivity using reflection method and coaxial probes. *Radio Engineering*, 17(1):14–19, 2008.